PHYSICAL REVIEW D **76,** 095001 (2007)

Constraining the two-Higgs-doublet-model parameter space

Abdul Wahab El Kaffas[*] and Per Osland[†]
Department of Physics and Technology, University of Bergen, Postboks 7803, N-5020 Bergen, Norway

Odd Magne Ogreid[‡]
Bergen University College, Bergen, Norway
(Received 24 June 2007; published 2 November 2007)

We confront the two-Higgs-doublet model with a variety of experimental constraints as well as theoretical consistency conditions. The most constraining data are the $\bar{B} \to X_s\gamma$ decay rate (at low values of $M_{H^\pm}$), and $\Delta\rho$ (at both low and high $M_{H^\pm}$). We also take into account the $B\bar{B}$ oscillation rate and R_b, or the width $\Gamma(Z \to b\bar{b})$ (both of which restrict the model at low values of $\tan\beta$), and the $B^- \to \tau\nu_\tau$ decay rate, which restricts the model at high $\tan\beta$ and low $M_{H^\pm}$. Furthermore, the LEP2 nondiscovery of a light, neutral-Higgs boson is considered, as well as the muon anomalous magnetic moment. Since perturbative unitarity excludes high values of $\tan\beta$, the model turns out to be very constrained. We outline the remaining allowed regions in the $\tan\beta$-$M_{H^\pm}$ plane for different values of the masses of the two lightest neutral-Higgs bosons, and describe some of their properties.

DOI: 10.1103/PhysRevD.76.095001 PACS numbers: 14.80.Cp

I. INTRODUCTION AND NOTATION

As compared with the standard model (SM), the two-Higgs-doublet model (2HDM) allows for an additional mechanism for CP violation [1–4]. This is welcome, in view of baryogenesis [5,6], and one of the main reasons for continued interest in the model.

Several experimental constraints restrict it. The B-$\bar{B}$ oscillations and branching ratio R_b exclude low values of $\tan\beta$, whereas the $\bar{B} \to X_s\gamma$ rate excludes low values of the charged-Higgs mass, $M_{H^\pm}$. The precise measurements at LEP of the ρ parameter constrain the mass splitting in the Higgs sector, and force the masses to be not far from the Z mass scale [7]. These individual constraints are all well known, but we are not aware of any dedicated attempt to combine them, other than those of [8,9]. The present study aims to go beyond that of [9], by using more complete and more up-to-date experimental results, as well as more accurate theoretical predictions for the above quantities.

From the theoretical point of view, there are also various consistency conditions. The potential has to be positive for large values of the fields [10,11]. We also require the tree-level Higgs-Higgs scattering amplitudes to be unitary [12–14]. Together, these constraints dramatically reduce the allowed parameter space of the model.

The present study is limited to the 2HDM (II), which is defined by having one Higgs doublet (Φ_2) couple to the up-type quarks, and the other (Φ_1) to the down-type quarks [15].

[*]awkaffas@ift.uib.no
[†]per.osland@ift.uib.no
[‡]omo@hib.no

We write the general 2HDM potential as

$$\begin{aligned} V = {} & \frac{\lambda_1}{2}(\Phi_1^\dagger\Phi_1)^2 + \frac{\lambda_2}{2}(\Phi_2^\dagger\Phi_2)^2 + \lambda_3(\Phi_1^\dagger\Phi_1)(\Phi_2^\dagger\Phi_2) \\ & + \lambda_4(\Phi_1^\dagger\Phi_2)(\Phi_2^\dagger\Phi_1) + \frac{1}{2}[\lambda_5(\Phi_1^\dagger\Phi_2)^2 + \text{H.c.}] \\ & - \frac{1}{2}\{m_{11}^2(\Phi_1^\dagger\Phi_1) + [m_{12}^2(\Phi_1^\dagger\Phi_2) + \text{H.c.}] \\ & + m_{22}^2(\Phi_2^\dagger\Phi_2)\}. \end{aligned} \tag{1.1}$$

Thus, the Z_2 symmetry will be respected by the quartic terms, and flavor-changing neutral currents are constrained [16]. We shall refer to this model (without the λ_6 and λ_7 terms) as the 2HDM$_5$. The more general model, with also λ_6 and λ_7 couplings, will be discussed elsewhere.

We allow for CP violation, i.e., λ_5 and m_{12}^2 may be complex. Thus, the neutral sector will be governed by a 3×3 mixing matrix, parametrized in terms of the angles α_1, α_2, and α_3 as in [4,17]:

$$R = \begin{pmatrix} c_1c_2 & s_1c_2 & s_2 \\ -(c_1s_2s_3 + s_1c_3) & c_1c_3 - s_1s_2s_3 & c_2s_3 \\ -c_1s_2c_3 + s_1s_3 & -(c_1s_3 + s_1s_2c_3) & c_2c_3 \end{pmatrix}, \tag{1.2}$$

where $c_1 = \cos\alpha_1$, $s_1 = \sin\alpha_1$, etc., and

$$-\frac{\pi}{2} < \alpha_1 \le \frac{\pi}{2}, \qquad -\frac{\pi}{2} < \alpha_2 \le \frac{\pi}{2}, \qquad 0 \le \alpha_3 \le \frac{\pi}{2}. \tag{1.3}$$

(In Ref. [17], the angles are denoted as $\tilde{\alpha} = \alpha_1$, $\alpha_b = \alpha_2$, $\alpha_c = \alpha_3$.) For a discussion of this parameter space, including the CP-nonviolating limits, see [18]. We will use the terminology "general 2HDM" as a reminder that CP

violation is allowed. The present study extends that of [9] also in this respect.

Rather than taking the parameters of the potential (1.1) to describe the model, we take the two lightest neutral-Higgs-boson masses, M_1 and M_2, together with the mixing angles (1.3), the charged-Higgs-boson mass, $M_{H^\pm}$, and $\tan\beta$ as our basic parameters. (The third neutral-Higgs-boson mass, M_3, is then a derived quantity.)

It is convenient to split the constraints into three categories:

(i) Theoretical consistency constraints: positivity of the potential [10,11] and perturbative unitarity [12–14],
(ii) Experimental constraints on the charged-Higgs sector. These all come from B-physics, and are due to $b \to s\gamma$, B-$\bar{B}$ oscillations, and $B \to \tau\nu_\tau$. They are all independent of the neutral sector.
(iii) Experimental constraints on the neutral sector. These are predominantly due to the precise measurements of R_b, nonobservation of a neutral-Higgs boson at LEP2, $\Delta\rho$, and $a_\mu = \frac{1}{2}(g-2)_\mu$.

The first and third categories of constraints will depend on the neutral sector, i.e., the neutral-Higgs masses and the mixing matrix. The second category is due to physical effects of the charged-Higgs Yukawa coupling in the B-physics sector. These are "general" in the sense that they do not depend on the spectrum of neutral-Higgs bosons, i.e., they do not depend on the mixing (and possible CP violation) in the neutral sector.

When considering the different experimental constraints, our basic approach will be that they are all in agreement with the standard model, and simply let the experimental or theoretical uncertainty restrict possible 2HDM contributions (this procedure yields lower bounds on the charged-Higgs mass, possibly also other constraints). An alternative approach would be to actually fit the 2HDM to the data. This will not be discussed in the present paper.

This paper is organized as follows. In Sec. II we discuss the general constraints of positivity of the Higgs potential, together with tree-level unitarity of Higgs-Higgs scattering amplitudes. The impact of these constraints is displayed in the $\tan\beta$-$M_{H^\pm}$ plane for a few representative values of neutral-Higgs-boson masses. Next, in Sec. III, we discuss the constraints coming from the B-physics experiments, in particular, the $\bar{B} \to X_s\gamma$, $B \to \tau\bar{\nu}_\tau$ and B-$\bar{B}$ oscillations. Section IV is devoted to various experimental constraints that depend on details of the neutral-Higgs sector. In Sec. V, we combine all the constraints and in Sec. VI we give some characteristics of the surviving parameter space. In Sec. VII we speculate on possible future experimental constraints, and then summarize in Sec. VIII.

II. GENERAL THEORY CONSTRAINTS

In the general CP-nonconserving case, the neutral sector is conveniently described by the three mixing angles, together with two masses (M_1, M_2), $\tan\beta$ and

$$\mu^2 = \frac{\mathrm{Re}\, m_{12}^2}{2\cos\beta\sin\beta}. \tag{2.1}$$

We shall here project these constraints from the multi-dimensional parameter space onto the $\tan\beta$-$M_{H^\pm}$ plane. Such a projection of information from a multidimensional space onto a point in the $\tan\beta$-$M_{H^\pm}$ plane can be done in a variety of ways, all of which will lead to some loss of information. However, we feel that this loss of detailed information can be compensated for by the "overview" obtained by the following procedure:

(1) Pick a set of neutral-Higgs-boson masses, (M_1, M_2) together with μ^2.
(2) Scan an $N = n_1 \times n_2 \times n_3$ grid in the α_1-α_2-α_3 space, and count the number j of these points that give a viable model. (Alternatively, one could scan over N random points in this space.)
(3) The ratio

$$Q = j/N, \qquad 0 \le Q \le 1, \tag{2.2}$$

is then a figure of merit, a measure of "how allowed" the point is, in the $\tan\beta$-$M_{H^\pm}$ plane. If $Q = 0$, no sampled point in the $\boldsymbol{\alpha} = (\alpha_1, \alpha_2, \alpha_3)$ space is allowed, if $Q = 1$, they are all allowed. An alternative measure

$$Q_+ = j/N_+, \qquad Q_+ \ge Q, \tag{2.3}$$

counts in the denominator only those points N_+ for which positivity is satisfied.

Of course the 2HDM, if realized in nature, would only exist at *one* point in this parameter space. However, we think the above quantities Q and Q_+ give meaningful measures of how "likely" different parameters are.

A. Reference masses

We shall impose the conditions of positivity, unitarity, and experimental constraints on the model, for the different "reference" mass sets given in Table I (and variations around these). For each of these mass sets we scan the model properties in the $\boldsymbol{\alpha} = (\alpha_1, \alpha_2, \alpha_3)$ space. (All scans have been performed over a $200 \times 200 \times 100$ grid. We note that other scanning procedures might be more efficient [19].) From these reference masses, some trends will emerge, allowing us to draw more general conclusions.

TABLE I. Reference masses.

Name	M_1 [GeV]	M_2 [GeV]	μ^2 [GeV^2]
"100–300"	100	300	$0[\pm(200)^2]$
"150–300"	150	300	$0[\pm(200)^2]$
"100–500"	100	500	$0[\pm(200)^2]$
"150–500"	150	500	$0[\pm(200)^2]$

In the 2HDM$_5$, with Im$\lambda_5 \neq 0$, the two input masses will together with $\boldsymbol{\alpha}$ and tanβ determine M_3 [17]. Specifying also $M_{H^\pm}$ and μ^2, all the λ's can be determined. (For explicit formulas, see [18].)

B. Positivity and unitarity

Let us first discuss the effect of imposing positivity. Actually, we will use the term "positivity" to refer to the nontrivial conditions $M_3^2 > 0$ and $M_2 \leq M_3$ together with $V(\Phi_1, \Phi_2) > 0$ as $|\Phi_1|, |\Phi_2| \to \infty$. We shall henceforth refer to the set of points in the $\boldsymbol{\alpha}$ space where positivity is satisfied, as $\boldsymbol{\alpha}_+$. In Table II of [18] we report percentages Q of points in $\boldsymbol{\alpha}$ space for which positivity is satisfied. For the mass parameters of Table I, the fraction is around 30%. For small and negative values of μ^2, "most" of the exclusion provided by the positivity constraint is due to the conditions $M_3^2 > 0$ and $M_3 > M_2$, without the explicit conditions on the λ's discussed, for example, in Appendix A of [11].

In Fig. 1, for $\mu^2 = 0$, we study the effects of imposing unitarity [12–14]. This has a rather dramatic effect at "large" values of tanβ and $M_{H^\pm}$. While the general constraints on the charged-Higgs sector, to be discussed in Sec. III, exclude low values of tanβ and $M_{H^\pm}$, the constraints of unitarity exclude high values of these same parameters. Only some region in the middle remains not excluded. For $(M_1, M_2) = (100, 300)$ GeV and $\mu^2 = 0$, unitarity excludes everything above tan$\beta \sim 5$ (for any value of $M_{H^\pm}$), and above $M_{H^\pm} \sim 650$ GeV (for any value of tanβ).

We shall refer to the set of $\boldsymbol{\alpha}$ values for which unitarity as well as positivity are satisfied as $\hat{\boldsymbol{\alpha}} \in \boldsymbol{\alpha}_+$. For $M_2 = 300$ GeV (upper panels), the percentage of points in $\boldsymbol{\alpha}_+$ space for which unitarity is satisfied, reaches (at low tanβ and low $M_{H^\pm}$) beyond 60%, whereas for $M_2 = 500$ GeV (lower panels), it only reaches values of the order of 15%–20%.

The domains in which $Q_+ > 0$ depend on μ^2: For negative values of μ^2, the region typically shrinks to lower values of tanβ, for positive values of μ^2 it extends to larger values of tanβ. When $\mu^2 \simeq 0$, and tan$\beta \leq 5$, significant fractions of the $\hat{\boldsymbol{\alpha}}$ space are allowed. However, for large positive values of μ^2, when also large values of tanβ are allowed, only small domains in $\hat{\boldsymbol{\alpha}}$ remain allowed, as

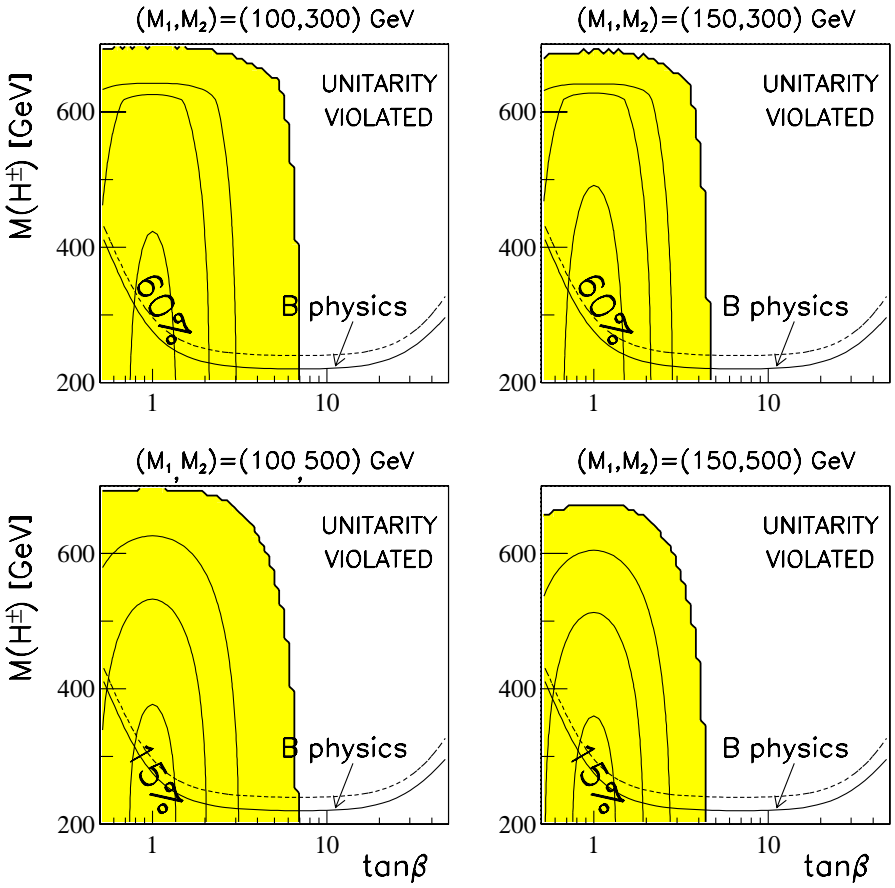

FIG. 1 (color online). Percentage of points Q_+ in the $\boldsymbol{\alpha}_+$ space that satisfy unitarity. Four sets of (M_1, M_2) values are considered, as indicated. The contours show $Q_+ = 0$, 20%, 40%, and 60% (upper panels) and 0, 5%, 10%, and 15% (lower panels). All panels: $\mu^2 = 0$. Yellow region: $Q_+ > 0$. Also shown, are the 90% (dashed line) and 95% (solid line) C.L. exclusion contours from Fig. 2.

discussed in [18]. They can actually be hard to find in a regular, equidistant scan over $\hat{\boldsymbol{\alpha}}$.

The unitarity constraints are conveniently formulated in terms of the different weak isospin and hypercharge channels [14]. At large values of $\tan\beta$ it turns out to be the isospin-zero, hypercharge-zero channel that is most constraining.

III. GENERAL CONSTRAINTS FROM THE $H^\pm$ SECTOR

The precise B-physics experiments provide severe constraints on the charged-Higgs sector, excluding low values of $M_{H^\pm}$ and $\tan\beta$. We shall here discuss the three most severe constraints of this kind that are independent of the neutral sector.

A. $\bar{B} \to X_s\gamma$

The $\bar{B} \to X_s\gamma$ branching rate was early found to constrain the allowed charged-Higgs-boson masses, but also to be very sensitive to QCD effects. At leading logarithmic order (LO), it is given by [20–22]:

$$\mathcal{B}(\bar{B} \to X_s\gamma) = \frac{|V_{ts}^* V_{tb}|^2}{|V_{cb}|^2} \frac{6\alpha_{\text{e.m.}}}{\pi g(z)} |C_7^{(0)\text{eff}}(\mu_b)|^2 \times \mathcal{B}(\bar{B} \to X_c e \bar{\nu}_e), \tag{3.1}$$

where the first factor is a ratio of Cabibbo-Kobayashi-Maskawa (CKM) matrix elements, $g(z = m_c^2/m_b^2)$ is a phase space factor, and $C_7^{(0)\text{eff}}(\mu_b)$ is an effective Wilson coefficient, evaluated at the B-meson scale, μ_b. This effective Wilson coefficient is obtained from the relevant ones at the electroweak scale, $C_i^{(0)}(\mu_0)$, $i = 2, 7, 8$ [23], where the effects of the 2HDM enter. Certain linear combinations are denoted "effective" coefficients, they are defined such that e.g. $C_7^{(0)\text{eff}}(\mu)$ includes all one-loop contributions to $b \to s\gamma$, i.e., also those of four-quark operators [23]. The effective Wilson coefficient was early found to be quite sensitive to the scale relevant to B-meson decay, changing by $\pm 25\%$ if the scale μ_b is varied by a factor of 2 in either direction around $m_b \simeq 5$ GeV [23,24]. At the NLO, this scale sensitivity is, however, significantly reduced [25–33].

The additional contributions due to the 2HDM can at the weak scale be described by diagrams involving $H^\pm$ exchange, and depend on this mass, $M_{H^\pm}$, as well as on the Yukawa couplings, i.e., on $\tan\beta$. At leading logarithmic order in QCD, they are discussed in [21,34]. Some of these additional terms can be enhanced by factors $\cot^2\beta$ from the $H^\pm$ Yukawa coupling squared. They all vanish linearly in $m_t^2/M_{H^\pm}^2$, i.e., for $M_{H^\pm}^2 \gg m_t^2$.

The NLO results for the 2HDM have been studied by many authors, see [30,31,35,36]. As compared with the LO calculation, it has been found that the NLO effects weaken the constraints on the allowed region in the $\tan\beta$-$M_{H^\pm}$ plane [23,35,36], the bound on $M_{H^\pm}$ is significantly relaxed.

Apart from minor effects, this calculation has for the SM been carried to the next-to-next-to-leading order (NNLO) [37]. At the NNLO, the branching ratio can be written as [31,38]:

$$\mathcal{B}(\bar{B} \to X_s\gamma) = \frac{|V_{ts}^* V_{tb}|^2}{|V_{cb}|^2} \frac{6\alpha_{\text{e.m.}}}{\pi C} \{P(E_0) + N(E_0)\} \times \mathcal{B}(\bar{B} \to X_c e \bar{\nu}_e)_{\text{exp}}, \tag{3.2}$$

where P and N denote perturbative and nonperturbative effects that both depend on the photon lower cutoff energy E_0. In the LO limit, the term P reduces to the square of the effective Wilson coefficient $C_7^{(0)\text{eff}}(\mu_b)$ in (3.1), whereas NLO and NNLO contributions include effects due to gluon exchange and emission, and require the summation over a bilinear expression involving also other Wilson coefficients. The factor C accounts for m_c-dependence associated with the semileptonic decay $\bar{B} \to X_c e \bar{\nu}_e$ [31].

The SM prediction of Misiak *et al.* is $(3.15 \pm 0.23) \times 10^{-4}$ for $E_0 = 1.6$ GeV [37,38], if all errors are added in quadrature. This is to be compared with the recent experimental results, which are averaged to 3.55×10^{-4} [39], with an uncertainty of 7%–7.5%, again with statistical and systematic errors added in quadrature. Andersen and Gardi [40] advocate a different approach to the resummation of the perturbation series, by "dressed gluon exponentiation," which accounts for multiple and soft collinear radiation. These effects are particularly important for large photon energies. Their approach yields $(3.47 \pm 0.48) \times 10^{-4}$, i.e., they find a 14% uncertainty. Becher and Neubert also introduce further corrections to the calculation of the photon spectrum, and find a rather low value, $(2.98 \pm 0.26) \times 10^{-4}$ [41], leaving more room for new physics.

The 2HDM contribution is positive, a finite value for the charged-Higgs mass would thus bring the results of [37,41] in closer agreement with the experiment. We shall, however, take the attitude that these numbers are compatible and compare the uncertainty in the experimental result and the SM prediction with the 2HDM contribution.

In the NNLO, the perturbative contribution P is obtained via the following three steps [38]:

(1) Evaluation of the Wilson coefficients at the "high" (electroweak) scale, μ_0 [42,43]. These coefficients are expanded to second order in α_s and rotated to effective Wilson coefficients $C_i^{\text{eff}}(\mu_0)$ [23,44]. The 2HDM effects enter at this stage, at lowest order in the Wilson coefficients $C_7(\mu_0)$ and $C_8(\mu_0)$.

(2) Evaluation of the "running" and mixing of these operators, from the high scale to the "low" (B-meson) scale. This is where the main QCD effects enter via a matrix U that is given in terms of powers of $\eta = \alpha_s(\mu_0)/\alpha_s(\mu_b)$ [23,28,44,45].

(3) Evaluation of matrix elements at the low scale

[38,46], which amounts to constructing $P(E_0)$ of Eq. (3.2) from the $C_i^{\rm eff}(\mu_b)$.

We adopt the scale parameters of [37]:

$$\mu_0 = 160\ \text{GeV}, \qquad \mu_b = 2.5\ \text{GeV}, \qquad \mu_c = 1.5\ \text{GeV}. \tag{3.3}$$

Actually, our treatment of the higher-order effects has been simplified compared to that described in [37,38], in the sense that: (i) We determine the contribution $P_2^{(2)\beta_0}$ of [38] by their Eq. (4.10), using results of [32,46,47], but read off $P_2^{(2)\rm rem} = 5$ (valid at the "default" scales) from their Fig. 2. (ii) Rather than explicitly including the $\mathcal{O}(V_{ub})$ and electroweak corrections, we adopt the corresponding numerical values of $+1\%$ [31,38] and -3.7% [31,48], respectively.

Furthermore, while the "matching" in the SM is performed to second order in α_s, we include, in addition to the dominant, lowest order, 2HDM effects, also the first-order (in $\alpha_s(\mu_0)$) contributions. In fact, we include the latter at the level of effective Wilson coefficients, following [36], and take their "matching scale" μ_W as μ_0. Characteristic relative magnitudes of the LO and NLO 2HDM contributions are given in Table II, for $\tan\beta = 1$ and 10, and $M_{H^\pm} = 300$ GeV and 600 GeV. The LO 2HDM contribution is measured with respect to the full SM value, whereas the NLO 2HDM contribution (according to [36]) is measured relative to the SM value plus the LO 2HDM contribution. The missing $\mathcal{O}(\alpha_s^2(\mu_0))$ corrections appear unimportant.

As input parameters for (3.2), in addition to (3.3), we take the CKM ratio to be 0.9676 [49], $\mathcal{B}(\bar{B} \to X_c e \bar{\nu}_e) = 0.1061$ [50] (see also [51]), $m_t(\mu_0) = 162$ GeV (corresponding to a pole mass of $m_t = 171.4$ GeV), $m_c(m_c) = 1.224$ GeV [52], and $m_b^{1S} = 4.68$ GeV [52], yielding $m_c(\mu_c) = 1.131$ GeV and $m_c(\mu_c)/m_b = 0.242$. For the nonperturbative part, $N(E_0)$, we follow Refs. [38,53,54]. Our result for the branching ratio, Eq. (3.2), in the SM limit ($M_{H^\pm} \to \infty$), is 3.12×10^{-4}. We collect in Table III the various values obtained by different authors.

We define a χ^2 measure of the amount by which the 2HDM would violate the agreement with the SM value,

$$\chi^2_{b\to s\gamma} = \frac{[\mathcal{B}(\bar{B} \to X_s\gamma)_{\rm 2HDM} - \mathcal{B}(\bar{B} \to X_s\gamma)_{\rm ref}]^2}{\{\sigma[\mathcal{B}(\bar{B} \to X_s\gamma)]\}^2}. \tag{3.4}$$

Here, $\mathcal{B}(\bar{B} \to X_s\gamma)_{\rm 2HDM}$ denotes the 2HDM prediction. As noted above, it will depend on $\tan\beta$ and $M_{H^\pm}$, whereas $\mathcal{B}(\bar{B} \to X_s\gamma)_{\rm ref}$ denotes a reference value, taken to be the averaged experimental value, 3.55×10^{-4} [39].

For the uncertainty that enters in (3.4), we adopt the value

$$\sigma[\mathcal{B}(\bar{B} \to X_s\gamma)] = 0.35 \times 10^{-4}, \tag{3.5}$$

which corresponds to the experimental and (SM) theoretical uncertainties [37] added in quadrature. For the 2HDM, the theoretical studies have not been carried to the same level of precision, but we recall that the 2HDM-specific NLO-level contributions only modify the overall branching ratios by $\mathcal{O}(5\%)$. These numbers give $\chi^2_{\rm min} = 1.52$.

With the above choice, we can determine exclusion regions in the $\tan\beta$-$M_{H^\pm}$ plane. Such regions are shown in Fig. 2 for $\chi^2 = 4.61$ and 5.99, corresponding to confidence levels of 90% and 95%, respectively, for 2 degrees of freedom ($\tan\beta$ and $M_{H^\pm}$). The obtained bound differs from that given by Misiak *et al.* [37] even though the branching ratio is reproduced to a reasonable precision. The reason is as follows. For compatibility with the treat-

TABLE II. Relative (in percent) 2HDM contributions to the branching ratio at LO and NLO (Borzumati and Greub).

	$\tan\beta = 1$		$\tan\beta = 10$	
$M_{H^\pm}$ [GeV]	LO	NLO	LO	NLO
600	18.2	−3.7	16.3	−3.5
300	41.8	−5.5	36.5	−5.1

TABLE III. Branching ratios $\mathcal{B}(\bar{B} \to X_s\gamma)$ and uncertainties in units of 10^{-4}, all for $E_\gamma > E_0 = 1.6$ GeV.

Authors	$\mathcal{B}$	σ	Reference
HFAG	3.55	$0.24 \pm \cdots$	[39]
M.M. *et al.*	3.15	0.23	[37]
J. A. & E. G.	3.47	0.48	[40]
T. B. & M. N.	2.98	0.26	[41]
Present work	3.12	—	

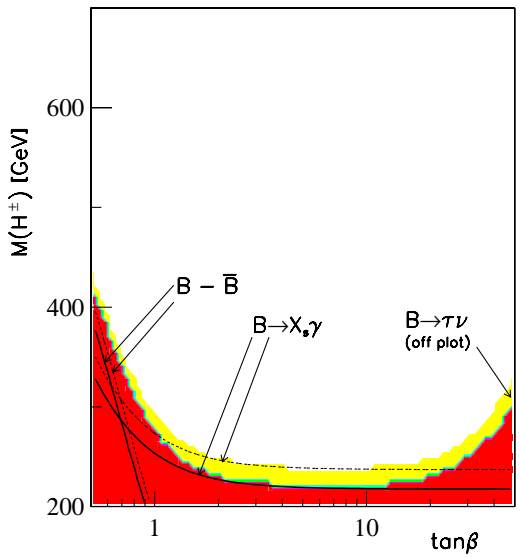

FIG. 2 (color online). Excluded regions at small $M_{H^\pm}$ and small $\tan\beta$ due to constraints from $\bar{B} \to X_s\gamma$ and B-$\bar{B}$ oscillations. Dashed: 90% C.L., solid: 95% C.L. The corresponding curves for $B \to \tau\nu$ are off the plot, to the lower right. Colored: joint exclusion at 90% and 95% C.L.

ment of the other experimental constraints, we consider a *two-dimensional* constraint, whereas they consider a single-sided one-dimensional constraint.[1]

By adopting the approximate SM-value $P_2^{(2)\mathrm{rem}} = 5$, we only include part of the 2HDM-specific contributions to $P^{(2)}$. A more well-defined procedure would be to leave out *all* 2HDM-specific contributions to $P^{(2)}$.[2] However, that procedure leads to an exclusion limit about 30 GeV higher in $M_{H^\pm}$, i.e., more of the parameter space would be excluded. We have chosen the more conservative approach, which leads to less exclusion.

B. $B \to X\tau\bar{\nu}_\tau$ and $B^- \to \tau\bar{\nu}_\tau$

Charged-Higgs bosons would contribute to the decay

$$b \to c\tau\bar{\nu}_\tau \tag{3.6}$$

from which the bound

$$\tan\beta < 0.52\ \mathrm{GeV} \times M_{H^\pm} \tag{3.7}$$

has been obtained [55] at the 2σ level. This bound, which would exclude a corner to the lower right outside the region shown in Fig. 2, is actually irrelevant, since such high values of $\tan\beta$ are excluded by the other constraints to be discussed in Sec. IV.

Charged-Higgs-boson exchange also contributes to

$$B^- \to \tau\bar{\nu}_\tau \tag{3.8}$$

which similarly provides a bound of the kind (3.7). The measurement gives $\mathcal{B}(B^- \to \tau\bar{\nu}_\tau) = (1.79 \pm 0.71) \times 10^{-4}$ [56], where we have added in quadrature symmetrized statistical and systematic errors. With a standard model prediction of $(1.59 \pm 0.40) \times 10^{-4}$,

$$r_{H\,\mathrm{exp}} = \frac{\mathcal{B}(B^- \to \tau\bar{\nu}_\tau)}{\mathcal{B}(B^- \to \tau\bar{\nu}_\tau)_{\mathrm{SM}}} = 1.13 \pm 0.53. \tag{3.9}$$

Interpreted in the framework of the 2HDM, one finds [55]

$$r_{H2\mathrm{HDM}} = \left[1 - \frac{m_B^2}{M_{H^\pm}^2}\tan^2\beta\right]^2. \tag{3.10}$$

We take $m_B = 5.28$ GeV, and formulate a χ^2 measure as

$$\chi^2_{b\to\tau\nu} = \frac{[r_{H2\mathrm{HDM}} - r_{H\,\mathrm{exp}}]^2}{[\sigma(r_{H\,\mathrm{exp}})]^2}. \tag{3.11}$$

It follows that two sectors at large values of $\tan\beta$ and low values of $M_{H^\pm}$ will be excluded. This bound is stronger than that of (3.7). It has some relevance in the lower right of Fig. 2, when all effects are added (see Sec. III D).

[1]We shall refer to $\chi^2 = 4.61$ and 5.99 as 90% and 95% C.L., respectively, even though this conversion to a probability only applies to the simple, ideal, case.

[2]We are grateful to M. Misiak for discussions on this and related issues.

C. B-$\bar{B}$ oscillations

The precisely measured B_d-$\bar{B}_d$ oscillations are at lowest order given by the formula [57]

$$\Delta m_{B_d} = \frac{G_F^2}{6\pi^2}|V_{td}^*|^2|V_{tb}|^2 f_B^2 B_B m_B \eta M_W^2 S_{2\mathrm{HDM}}, \tag{3.12}$$

with the Inami-Lim functions [58]

$$S_{2\mathrm{HDM}} = S_{WW} + 2S_{WH} + S_{HH}. \tag{3.13}$$

The contributions proportional to diagrams with the exchange of one or two charged-Higgs bosons are denoted S_{WH} and S_{HH}. They are proportional to $\cot^2\beta$ and $\cot^4\beta$, and vanish when $M_{H^\pm} \gg m_t$, as $(m_t^2/M_{H^\pm}^2)\log(m_t^2/M_{H^\pm}^2)$ and $m_t^2/M_{H^\pm}^2$, respectively.

At the NLO, the corresponding result has also been obtained [59]: B_B and η (denoted η_2 in [59]) receive corrections of order α_s. In particular, the $\mathcal{O}(\alpha_s)$ contribution to η_2 becomes a nontrivial function of $\tan\beta$ and $M_{H^\pm}$. A few comments are in order here: (i) The factor of 2 for the second term in (3.13) has been adopted to follow the notation of [59]. (ii) There is a bookkeeping problem with the expression for $L^{(i,H)}$ in Eq. (A.20) of [59]. Since the last term in that expression, proportional to a quantity denoted HH, has an explicit coefficient $1/\tan^4\beta$, the S_{HH} in Eqs. (A.21) and (A.24) for $HH^{(i)}$ should be replaced by $\tan^4\beta \times S_{HH}$. (iii) There is a discrepancy in a quantity denoted $2WW_{tu}^{(8)}$, between Eq. (A.16) in [59] and the later Ph.D. thesis of the same author. We have chosen to take the formula given in the thesis. At the level of η_2, it amounts to a difference of the order of 2%.[3]

The $\mathcal{O}(\alpha_s)$ corrections to η introduce a variation of η (or η_2) from 0.334 at $\tan\beta = 0.5$ and $M_{H^\pm} = 200$ GeV to 0.552 at $\tan\beta = 50$. (We have adopted the overall normalization of η such that it agrees with the SM value 0.552 [60] at $\tan\beta = 50$.) However, the product $\eta \times S_{2\mathrm{HDM}}$ varies by a factor of 2.7 over this same range, as compared with a factor of 4.5 for $S_{2\mathrm{HDM}}$ itself. Thus, the inclusion of the $\mathcal{O}(\alpha_s)$ QCD corrections reduces the sensitivity of Δm_B to charged-Higgs contributions. In other words, the inclusion of NLO corrections weakens the constraints on the 2HDM at low values of $\tan\beta$.

Recently, also the B_s-$\bar{B}_s$ oscillation parameter Δm_{B_s} has been measured [61]. It is given by an expression similar to (3.12), except that the CKM matrix elements are different:

$$\Delta m_{B_s} = \frac{G_F^2}{6\pi^2}|V_{ts}^*|^2|V_{tb}|^2 f_B^2 B_B m_B \eta M_W^2 S_{2\mathrm{HDM}}, \tag{3.14}$$

and $f_B^2 B_B$ and m_B, now referring to B_s, are numerically different.

The quantities $f_B B_B^{1/2}$ that appear in (3.12) and (3.14) are determined from lattice QCD studies, and rather uncertain.

[3]We are grateful to A. Buras, U. Jentschura, and F. Krauss for correspondence on these points (ii) and (iii).

We shall use the values adopted recently by Ball and Fleischer [60],

$$f_{B_d} B_{B_d}^{1/2} = (0.244 \pm 0.026)\ \text{GeV}, \qquad f_{B_s} B_{B_s}^{1/2} = (0.295 \pm 0.036)\ \text{GeV}, \tag{3.15}$$

based on unquenched calculations. In fact, these uncertainties are the dominant ones.

For each of these observables, one can form a χ^2 measure of the deviation from the SM:

$$\chi^2_{B_q-\bar{B}_q} = \frac{(\Delta m_{B_q 2\text{HDM}} - \Delta m_{B_q \text{SM}})^2}{[\sigma(\Delta m_{B_q})]^2}. \tag{3.16}$$

We adopt the attitude that the measurements of Δm_{B_d} and Δm_{B_s} furnish determinations of the CKM matrix elements $|V_{td}|$ and $|V_{ts}|$ that are compatible with the SM, and simply require that the additional 2HDM contributions do not spoil this consistency. With the assumption that the uncertainties in (3.15) are the dominant ones, we have

$$\sigma(\Delta m_{B_d}) = 21\% \times \Delta m_{B_d}, \qquad \sigma(\Delta m_{B_s}) = 24\% \times \Delta m_{B_s}. \tag{3.17}$$

However, with the theory error (3.15) being the dominant one, we cannot claim that the measurements of Δm_{B_d} and Δm_{B_s} furnish independent constraints on the model. Therefore, we consider only the χ^2 contribution from the more constraining one of these two measurements, namely Δm_{B_d} with a 21% uncertainty:

$$\chi^2_{B\text{-}\bar{B}} = \chi^2_{B_d\text{-}\bar{B}_d}. \tag{3.18}$$

Contours of $\chi^2_{B\text{-}\bar{B}}$ are shown in Fig. 2. As mentioned above, they are more generous than the corresponding bounds based on the LO theory.

D. Combining general constraints from the $H^\pm$ sector

In order to quantify the extent to which a particular point in the $\tan\beta$-$M_{H^\pm}$ plane is forbidden, we form a χ^2 as follows:

$$\chi^2_{\text{general}} = \chi^2_{b\to s\gamma} + \chi^2_{b\to\tau\nu} + \chi^2_{B\text{-}\bar{B}}. \tag{3.19}$$

The subscript "general" refers to the fact that constraints depending on the neutral sector are not yet taken into account. Yet, no choice of neutral-sector parameters can avoid these constraints.

Figure 2 shows excluded regions in the $\tan\beta$-$M_{H^\pm}$ plane, due to the constraints of $\bar{B} \to X_s\gamma$, $B^- \to \tau\bar{\nu}_\tau$, and B-$\bar{B}$ oscillations at 90% (dashed line) and 95% C.L. (solid line), as well as combined (indicated in yellow [light gray] and red [dark gray] at 90% and 95% C.L., respectively). Earlier versions of such exclusion plots can be found in [8,9,31].

IV. EXPERIMENTAL CONSTRAINTS ON THE NEUTRAL SECTOR

We now turn to the constraints coming from experiments related to the neutral-Higgs sector. These are not general, they will depend on the parameters of this sector, namely, neutral-Higgs masses and mixing angles. We will study, as representative cases, those given in Table I.

A problem with point 2 of the procedure of Sec. II, is the following. The conditions of positivity and unitarity are absolute,[4] with a certain fraction Q_+ of the points in the $\boldsymbol{\alpha}_+$ space satisfying these, whereas the experimental constraints are statistical, i.e., a certain parameter point may violate an experimental observation by 1σ, 2σ, or more. There is no obvious way to combine this information.

As a first step, we will consider one of these experimental constraints on the neutral sector at a time, and display the way it excludes parts of the $\tan\beta$-$M_{H^\pm}$ plane by the following simple consideration. Let χ^2_i be the contribution to χ^2 due to a particular experimental observable $\mathcal{O}_i$:

$$\chi^2_i = \frac{(\mathcal{O}_{i,2\text{HDM}} - \mathcal{O}_{i,\text{ref}})^2}{[\sigma(\mathcal{O}_i)]^2}, \tag{4.1}$$

where the reference value $\mathcal{O}_{i,\text{ref}}$ will be either the experimental value or the SM value.

We shall consider the following observables: R_b, the branching ratio for $Z \to b\bar{b}$ [62] (in Sec. IV A); the LEP2 nondiscovery of a light neutral-Higgs boson [63,64] (in Sec. IV B); ρ, the LEP determination of the relation between the Z and W masses [65] (in Sec. IV C); and $a_\mu = \frac{1}{2}(g-2)_\mu$, the precise Brookhaven determination of the muon anomalous magnetic moment [66] (in Sec. IV D). Then, the criterion we will consider in this first step, can be expressed in terms of the following quantity:

(i) For fixed $\tan\beta$ and $M_{H^\pm}$ take

$$\hat{\chi}^2_i = \min_{\hat{\boldsymbol{\alpha}} \in \boldsymbol{\alpha}_+} \chi^2_i, \tag{4.2}$$

where χ^2_i is minimized over the part $\hat{\boldsymbol{\alpha}}$ of the $\boldsymbol{\alpha}_+$ space for which positivity and also unitarity are satisfied.

The minimization over $\hat{\boldsymbol{\alpha}}$ finds the point where the model can most easily accommodate the particular experimental constraint, with the chosen masses (M_1, M_2) and μ^2 fixed. This point in $\hat{\boldsymbol{\alpha}}$ will in general differ from one experimental constraint to another. We will establish 90% and 95% C.L. allowed regions in the $\tan\beta$-$M_{H^\pm}$ plane, corresponding to one of these observables at a time. These will subsequently be combined. However, the overall allowed regions will in general be less than the intersection of the individual ones, since the latter will correspond to different points in $\hat{\boldsymbol{\alpha}}$.

[4] One might consider models for which perturbative unitarity is not satisfied, but we shall not do that here.

This procedure preserves none of the probabilistic information of Fig. 1, which shows that some region of the $\tan\beta$-$M_{H^\pm}$ plane contains more possible solutions than some other region. All focus is here on the one "best" point in $\boldsymbol{\alpha}$, where χ^2 is lowest.

A. R_b constraint (LEP)

The 2HDM-specific contributions to R_b are of two kinds. At low values of $\tan\beta$, the exchange of charged-Higgs bosons is important, whereas at high values of $\tan\beta$ the exchange of neutral-Higgs bosons is important [67]. For the general CP nonconserving case, the latter contributions are given in [11].

For this observable, the reference value in (4.1) is not well defined, since R_b [68] is part of the electroweak observables from which a SM Higgs mass is fitted. Hence, we take

$$\chi^2_{R_b} = \left(\frac{\Delta R_{b,\mathrm{2HDM}}}{\sigma(R_b)}\right)^2, \tag{4.3}$$

where $\Delta R_{b,\mathrm{2HDM}}$ refers to the 2HDM-specific contributions to this quantity [11,67] and with $\sigma(R_b) = 0.05\%$ the experimental uncertainty [62].

We show in Fig. 3, for two sets of (M_1, M_2) values, and $\mu = 0$, how this constraint removes a sliver of low-$\tan\beta$ values. The allowed regions are here cut off at $\tan\beta \gtrsim 7$ due to the unitarity constraint discussed in Sec. II B. The neutral-Higgs-exchange contribution to R_b is in this case of no importance.

Next, we show in Fig. 4, the corresponding allowed regions for $\mu = 200$ GeV. The large-$\tan\beta$ region is then less constrained by the unitarity constraints, but for the higher value of M_2 (right panel) the R_b modification that is caused by neutral-Higgs exchange starts to exclude high values of $\tan\beta$.

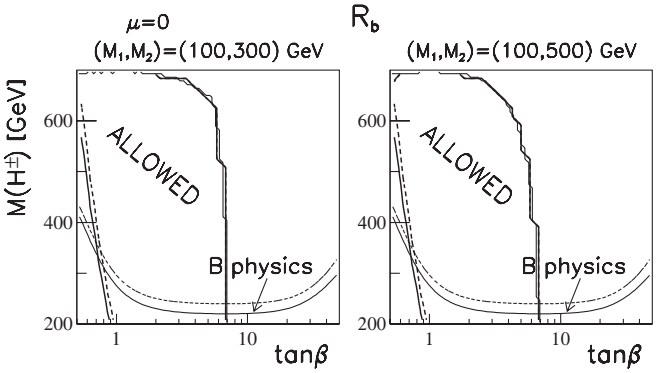

FIG. 3. Exclusions due to the ΔR_b constraint, $\hat{\chi}^2_{R_b}$, for $(M_1, M_2) = (100, 300)$ GeV and (100, 500) GeV, both for $\mu = 0$. Also shown is the region excluded by the B-physics constraints, and the 0% contour from Fig. 1 (thin upper right). Dashed: 90% C.L.; solid: 95% C.L.

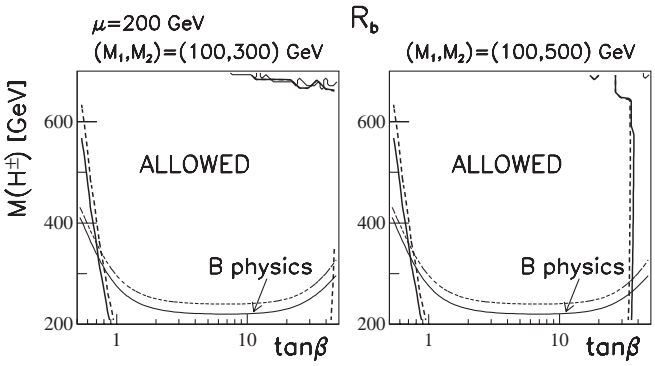

FIG. 4. ΔR_b constraint, similar to Fig. 3, for $\mu = 200$ GeV.

B. LEP2 nondiscovery

The nondiscovery of a neutral-Higgs boson at LEP2 is relevant only for $M_1 < 114.4$ GeV [62]. However, it is well known that these searches do not exclude certain other light neutral-Higgs bosons, if they couple more weakly to the Z boson, or if they decay to final states that are more difficult to detect and identify.

The constraint is implemented in an approximate way as follows. Following [63] (see also [64]), we consider the searches for a neutral-Higgs boson that decays to $b\bar{b}$ jets or a tau pair. Thus, the quantity of interest is the product of the production cross section (proportional to the square of the ZZH_1 coupling) and the $b\bar{b}$ (or $\tau^+\tau^-$) branching ratio (proportional to the square of the $H_1 b\bar{b}$ coupling). We denote the reduced sensitivity, as compared to the SM sensitivity, a "dilution factor" C^2 [63]:

$$\sigma_{\mathrm{2HDM}}(ZH_1 \to Zb\bar{b}) = \sigma_{\mathrm{SM}}(Zh \to Zb\bar{b}) \times C^2(ZH_1 \to Zb\bar{b}), \tag{4.4}$$

where the dilution factor is the product of a factor $C^2(ZH_1)$ related to the production and another, $C^2(H_1 \to b\bar{b})$, related to the branching ratio:

$$C^2(ZH_1 \to Zb\bar{b}) = C^2(ZH_1) \times C^2(H_1 \to b\bar{b}). \tag{4.5}$$

For the general 2HDM, $C^2(ZH_1 \to Zb\bar{b}) \equiv C^2_{\mathrm{2HDM}}$ is given by Eq. (4.3) in [11]. It depends on the neutral-sector rotation angles, as well as on $\tan\beta$, and is the same for $b\bar{b}$ and $\tau^+\tau^-$ final states.

As experimental constraints, we approximate the 95% C.L. bounds obtained in [63] by linear interpolations passing through the points given in Table IV, and form the *ad hoc* single-sided χ^2 penalty (summed over $b\bar{b}$ and $\tau^+\tau^-$):

TABLE IV. Experimental suppression factors C^2_{exp} [63].

M_1	80 GeV	100 GeV	114.4 GeV
$b\bar{b}$	0.06	0.25	1.0
$\tau^+\tau^-$	0.06	0.2	1.0

$$\chi^2_{\rm LEP2} = 5.99\left(\frac{C^2_{\rm 2HDM} - C^2_{\rm exp}}{1 - C^2_{\rm exp}}\right)^2 \qquad (4.6)$$

for $C^2_{\rm 2HDM} > C^2_{\rm exp}$ and $M_1 < 114.4$ GeV, and zero otherwise. The coefficient 5.99 corresponds to 95% probability in the context of our two "degrees of freedom," $\tan\beta$ and $M_{H^\pm}$.

We show in Fig. 5 the resulting exclusion for $M_1 = 100$ GeV, $\mu = 0$ and two values of M_2 as indicated. For the higher value of M_2, we note that some part of the otherwise allowed parameter space gets excluded. Given that $C^2_{\rm 2HDM}$ is determined by $\tan\beta$ and the $\boldsymbol{\alpha}$ parameters, one might wonder why this excluded region depends also on $M_{H^\pm}$. The reason is of course that the subspace of $\boldsymbol{\alpha}$ that is allowed by the positivity and unitarity constraints depends on $M_{H^\pm}$, and need not overlap with the corresponding subspace of $\boldsymbol{\alpha}$ for which $C^2_{\rm 2HDM}$ is within the allowed range.

For $\mu = 200$ GeV (Fig. 6), the unitarity constraints no longer exclude high values of $\tan\beta$, but we see that the LEP nondiscovery excludes high values of charged-Higgs mass (via its impact on the rotation matrix). In fact, at large values of $\tan\beta$, if $M_1 < 114.4$ GeV, the LEP2 nondiscovery requires (see Eq. (4.3) of [11])

$$\frac{1}{\cos^2\beta} R^2_{12}[R^2_{11} + R^2_{13}] < 1. \qquad (4.7)$$

For small values of $\cos\beta$, this is satisfied in three separate regions [see Eq. (1.2) and figures of Sec. VI]:

$$\begin{aligned} &\text{(i): } \alpha_1 \simeq 0, \qquad \text{(ii): } |\alpha_2| \simeq \pi/2, \\ &\text{(iii): } |\alpha_1| \simeq \pi/2 \quad \text{and} \quad \alpha_2 \simeq 0. \end{aligned} \qquad (4.8)$$

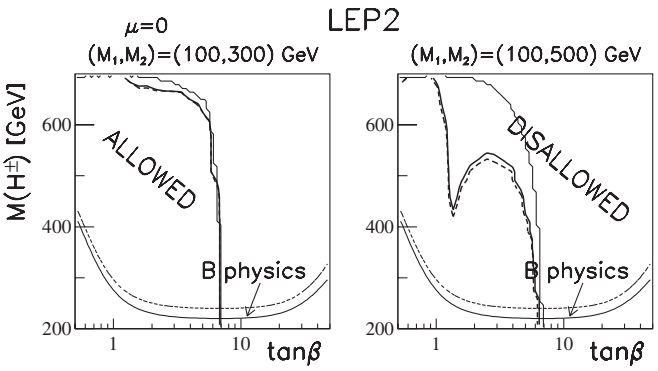

FIG. 5. Exclusions due to the LEP2 constraint, $\hat{\chi}^2_{\rm LEP2}$. Left: $(M_1, M_2) = (100, 300)$ GeV; Right: $(M_1, M_2) = (100, 500)$ GeV, $\mu = 0$ in both cases. Also shown is the region excluded by the B-physics constraints, and the 0% contour from Fig. 1 (thin upper right). Dashed: 90% C.L.; solid: 95% C.L.

C. The ρ parameter

The ρ parameter, defined as

$$\rho = \frac{M^2_W}{M^2_Z \cos^2\theta_{\rm W}}, \qquad (4.9)$$

is very sensitive to fields that couple to the W and Z [65]. Experimentally, ρ is constrained as [68]

$$\rho_{\rm exp} = 1.0050 \pm 0.0010. \qquad (4.10)$$

The deviation from unity is mostly due to the top-quark one-loop contributions, but there is also a weak dependence on the SM Higgs mass. In order to extract this quantity from the data, one fits for a SM Higgs mass, the contribution of which should then be subtracted from the 2HDM prediction.

The additional Higgs fields of the 2HDM can easily spoil the agreement with the SM [7]. Roughly speaking, this constraint requires the Higgs masses to be not too far from the W and Z masses, and not very much apart. For the general CP-nonconserving 2HDM, the results of [7] for the contributions to ρ, denoted $\Delta\rho = \rho_{\rm 2HDM} - \rho_{\rm SM}$, were generalized in [11] and given by Eqs. (4.8), (4.9), (4.10), (4.11), and (4.12) there.

In order to study this constraint, we evaluate χ^2_ρ as defined by

$$\chi^2_\rho = \left(\frac{\Delta\rho_{\rm 2HDM}}{\sigma(\rho)}\right)^2, \qquad (4.11)$$

with $\sigma(\rho) = 0.0010$, subtracting the SM contribution corresponding to a SM Higgs mass $M_0 = 129$ GeV.

In Figs. 7 and 8 we show the impact of $\hat{\chi}^2_\rho$ in constraining the parameter space for $\mu = 0$ and $\mu = 200$ GeV, respectively. At the higher value of M_2, and high values of $\tan\beta$, this constraint tends to exclude both low and high values of $M_{H^\pm}$. The irregular boundaries seen in Fig. 8 are obviously due to the scanning not finding the whole allowed region. (At high μ and high $\tan\beta$, only very tiny regions in α_1 and α_2 are allowed [18].)

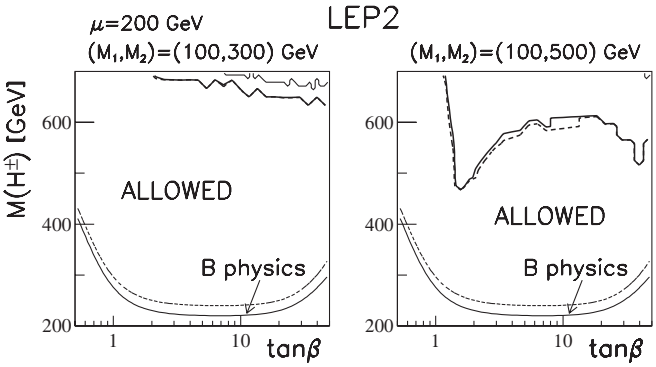

FIG. 6. LEP2 constraint, $\hat{\chi}^2_{\rm LEP2}$. Similar to Fig. 5, for $\mu = 200$ GeV.

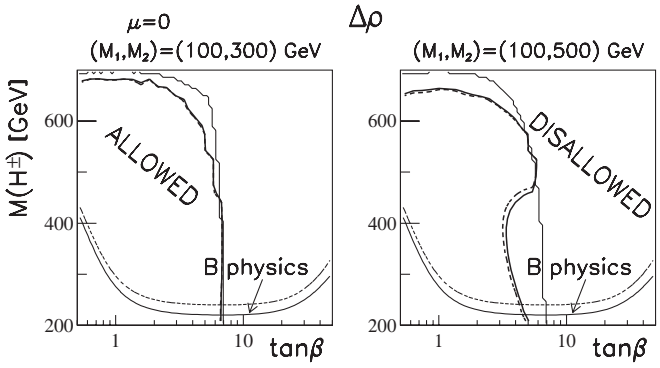

FIG. 7. Exclusions due to the $\Delta\rho$ constraint, $\hat{\chi}^2_\rho$. Left: $(M_1, M_2) = (100, 300)$ GeV; Right: $(M_1, M_2) = (100, 500)$ GeV, $\mu = 0$ in both cases. Also shown is the region excluded by the B-physics constraints, and the 0% contour from Fig. 1 (thin upper right). Dashed: 90% C.L.; solid: 95% C.L.

It is instructive to consider the contribution to $\Delta\rho$ in the limit of large values of $\tan\beta$. The expressions (4.10) and (4.12) of [11] simplify considerably in the limit $\sin\beta \to 1$, and provide an understanding of features seen in Figs. 7 and 8:

$$A^{HH}_{WW}(0) - \cos^2\theta_W A^{HH}_{ZZ}(0) \to \frac{g^2}{64\pi^2}\sum_j \Big[(R^2_{j1} + R^2_{j3}) \times F_{\Delta\rho}(M^2_{H^\pm}, M^2_j) - \sum_{k>j} (R_{j1}R_{k3} - R_{k1}R_{j3})^2 F_{\Delta\rho}(M^2_j, M^2_k) \Big], \tag{4.12}$$

and

$$A^{HG}_{WW}(0) - \cos^2\theta_W A^{HG}_{ZZ}(0) \to \frac{g^2}{64\pi^2}\Big[\sum_j R^2_{j2}(3F_{\Delta\rho}(M^2_Z, M^2_j) - 3F_{\Delta\rho}(M^2_W, M^2_j)) + 3F_{\Delta\rho}(M^2_W, M^2_0) - 3F_{\Delta\rho}(M^2_Z, M^2_0) \Big] \tag{4.13}$$

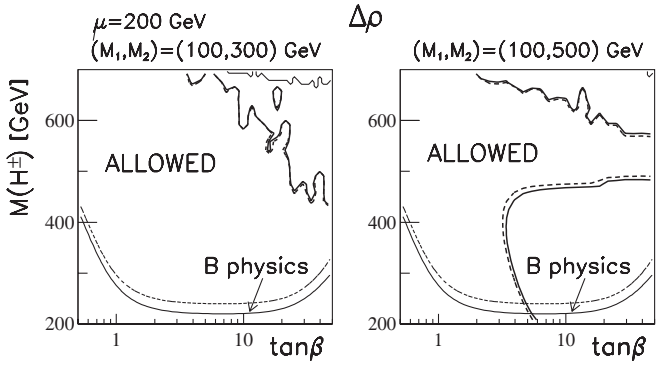

FIG. 8. Exclusions due to the $\Delta\rho$ constraint, $\hat{\chi}^2_\rho$. Similar to Fig. 7, for $\mu = 200$ GeV.

with $F_{\Delta\rho}(m^2_1, m^2_2)$ found in Eq. (4.11) of [11]. This function vanishes when the two masses are equal, and grows quadratically with the bigger of the two masses. The contribution given by (4.13) is rather small, since M_Z and M_W are relatively close.

The only part sensitive to the charged-Higgs mass is the first sum in (4.12), which may, however, get significant contributions from all three neutral-Higgs bosons, $j = 1$, 2, 3. Consider first the contribution from H_1. Barring cancellations (see below), a viable parameter point must for large $\tan\beta$ and large $M^2_{H^\pm} \gg M_1$ have

$$R^2_{11} + R^2_{13} \ll 1. \tag{4.14}$$

Expressed in terms of the angles, this means that $c^2_1 c^2_2 + s^2_2 \ll 1$, or

$$|\alpha_1| \sim \pi/2 \quad \text{and} \quad \alpha_2 \sim 0. \tag{4.15}$$

Note that this condition is compatible with (4.7) and corresponds to case (iii) of (4.8).

Next, we consider the case (with increasing splitting between M_2 and M_3, the contribution to $\Delta\rho$ will increase)

$$M_{H^\pm} \ll M_2 \simeq M_3, \tag{4.16}$$

then again barring cancellations, the $\Delta\rho$ condition requires

$$\sum_{j=2}^{3}(R^2_{j1} + R^2_{j3}) = c^2_1 s^2_2 + s^2_1 + c^2_2 \ll 1. \tag{4.17}$$

This condition *cannot* be satisfied, and low values of $M_{H^\pm}$ are thus excluded when $\tan\beta$ is large and M_2 is large.

For high values of $M_{H^\pm}$, the most sensitive contribution is that involving H_1. But unless $M_{H^\pm}$ is close to M_2, the condition (4.15), related to the H_1 contribution, is not sufficient. The H_2 and H_3 contributions are proportional to $R^2_{21} + R^2_{23}$ and $R^2_{31} + R^2_{33}$, respectively. In the limit (4.15), these are both equal to 1, i.e., when the rotation matrix is adjusted such as to cancel the H_1 contribution to the first sum in (4.12), there is no suppression of the H_2 and H_3 contributions. As a result, such high values of $M_{H^\pm}$ are forbidden.

An exception to this situation arises when μ is large compared with M_2. Then, there can be a considerable splitting between M_2 and M_3, $M_{H^\pm}$ and M_3 can be similar, and a cancellation between the $(M_1, M_{H^\pm})$ and the (M_1, M_3) terms of (4.12) is possible. As a result, for large values of μ, large values of $M_{H^\pm}$ can be allowed.

Finally, we consider the situation

$$M_1 \ll M_2 \simeq M_3 \simeq M_{H^\pm}, \tag{4.18}$$

which applies to the "finger" protruding to the right in the right panel of Fig. 8. Then, the contributions of the two sums in Eq. (4.12) tend to cancel. For $j = 1$ and $k = 2, 3$, we get

$$[R_{11}^2 + R_{13}^2 - (R_{11}R_{23} - R_{21}R_{13})^2 - (R_{11}R_{33} - R_{31}R_{13})^2]F_{\Delta\rho}(M_1^2, M_2^2) = 0, \quad (4.19)$$

where we have used the orthogonality of the rotation matrix. Thus, when $\tan\beta$ is large, and $M_2 \simeq M_3 \simeq M_{H^\pm}$, there is a cancellation among the terms in (4.12), only the (small) (4.13) part of the $\Delta\rho$ constraint is relevant.

D. Muon anomalous magnetic moment a_μ

The precisely measured muon anomalous magnetic moment [66],

$$a_{\mu,\mathrm{exp}} \equiv \tfrac{1}{2}(g-2)_{\mu,\mathrm{exp}} = 11\,659\,208(5.4)(3.3) \times 10^{-10} \quad (4.20)$$

is a sensitive probe of new physics (for a recent review, see [69]). The statistical and systematic uncertainties (given in parentheses) combine to an overall uncertainty of 6.3×10^{-10}. The corresponding SM prediction, including weak and strong effects, is [69]

$$a_{\mu,\mathrm{SM}} = 11\,659\,179.3(6.8) \times 10^{-10}, \quad (4.21)$$

creating a 3σ "tension" with the experimental result.

In the 2HDM, there are additional contributions, dominated by the two-loop Barr-Zee effect [70] with a photon and a Higgs field connected to a heavy-fermion loop. For the CP-conserving case, the contribution is given by [9,71]. For the general (CP-violating) 2HDM, the top-quark contribution to a_μ for the muon, is given by Eq. (4.13) in [11], whereas the b-quark contribution to the fermion loop is given by

$$\Delta a_\mu = \frac{N_c \alpha_{\mathrm{e.m.}}}{4\pi^3 v^2} m_\mu^2 Q_b^2 \sum_j \left[\tan^2\beta R_{j3}^2 g\left(\frac{m_b^2}{M_j^2}\right) - \frac{1}{\cos^2\beta} R_{j1}^2 f\left(\frac{m_b^2}{M_j^2}\right)\right], \quad (4.22)$$

with $N_c = 3$ the number of colors associated with the fermion loop, $\alpha_{\mathrm{e.m.}}$ the electromagnetic fine structure constant, $Q_b = -1/3$ and m_b the b-quark charge and mass, and m_μ the muon mass. The τ-loop contribution, which we also include, is given by a similar expression, with obvious substitutions for the color factor, charge, and mass. The functions f and g are given in [70].

At low values of $\tan\beta$, these contributions are negligible, but the b- and τ-loop contributions can become relevant at very large values of $\tan\beta$. As a measure of the possible conflict with the 2HDM, we consider

$$\chi^2_{a_\mu} = \left(\frac{\Delta a_{\mu,\mathrm{2HDM}}}{\sigma(a_\mu)}\right)^2, \quad (4.23)$$

where $\Delta a_{\mu,\mathrm{2HDM}}$ is the 2HDM-specific contribution, and for the uncertainty we take the (SM) theoretical value, $\sigma(a_\mu) = 6.8 \times 10^{-10}$, since this is larger than the experimental one.

Actually, this constraint does not have any significant impact within the range of $\tan\beta$ considered. Let us consider its "natural value" as that contributed by one of the two terms in (4.22), with the rotation matrix element set to 1. This reaches $\chi^2 = \mathcal{O}(1)$ for $\tan\beta$ of the order of 70. However, there can be significant reductions by the rotation matrix elements, and also cancellations among the two terms. At such high values of $\tan\beta$ the $B \to \tau\nu_\tau$ constraint (see Sec. III B) is important at low values of $M_{H^\pm}$, and the unitarity constraint may be important at high $M_{H^\pm}$ (depending on the relative magnitude of M_2 and μ).

We recall that at high $\tan\beta$, the rotation matrix is rather constrained by unitarity [18]. Let us focus on the contribution of the lightest neutral-Higgs boson, H_1, whose contributions to (4.22) are given by R_{11}^2 and R_{13}^2. Thus, in spite of the enhancement given by the $\tan\beta$-dependent factors, this contribution to a_μ may be small if

$$|\alpha_1| \sim \pi/2 \quad \text{and} \quad \alpha_2 \sim 0. \quad (4.24)$$

In the limit of large $\tan\beta$ and large $M_{H^\pm}$, this is actually the only region allowed by the $\Delta\rho$ constraint, see Eq. (4.15). We conclude that at large $\tan\beta$ and large $M_{H^\pm}$, the a_μ constraint is covered by the $\Delta\rho$ constraint. But this coefficient $R_{11}^2 + R_{13}^2$ arises in one case from the Yukawa couplings, and in the other from the gauge-Higgs couplings. Furthermore, at large $\tan\beta$ and moderate $M_{H^\pm}$ values, the a_μ constraint is covered by the $B \to \tau\nu_\tau$ constraint.

E. Summary on neutral-sector constraints

We will here summarize the conclusions on the neutral-sector constraints, treating first the simpler case of $\mu = 0$ (where $\tan\beta$ is bounded), and next comment on the less restrictive case of large μ (where also larger values of $\tan\beta$ are allowed). The R_b constraint is at low values of $\tan\beta$ dominated by the charged-Higgs-exchange contribution. This part of the R_b constraint is thus independent of the neutral sector.

1. The case $\mu = 0$

For $\mu = 0$, and $(M_1, M_2) = (100, 300)$ GeV, the only neutral-sector constraint that has some impact, apart from R_b at low values of $\tan\beta$, is the $\Delta\rho$ constraint, which excludes the higher range of $M_{H^\pm}$, as illustrated in the left panel of Fig. 7. However, for $M_2 = 500$ GeV, other constraints are also important. The LEP2 nondiscovery rules out large values of $\tan\beta$ and $M_{H^\pm}$, and to some extent, also the $\Delta\rho$ constraint rules out some region of large $\tan\beta$.

However, with $\mu = 0$, high values of $\tan\beta$ are also excluded by the unitarity constraints, and, to some extent, the low values of $M_{H^\pm}$ are excluded by the B-physics constraints.

2. The case $\mu > M_1$

When $\mu > M_1$, large values of $\tan\beta$ become accessible. This parameter region is known as the decoupling region [72]. We here distinguish two cases

$$\text{(i) } M_1 < \mu < M_2, \qquad \text{(ii) } M_1 < M_2 < \mu. \tag{4.25}$$

.

The R_b constraint, which at low $\tan\beta$ is dominated by the charged-Higgs contributions, can at large $\tan\beta$ also exclude some region of neutral-Higgs-boson mass values (compare the left and right panels of Fig. 4). Furthermore, the LEP2 constraint may exclude high values of $M_{H^\pm}$ (see right panel of Fig. 6) and the $\Delta\rho$ constraint may at high $\tan\beta$ constrain the range of $M_{H^\pm}$ values to a band around M_2.

V. COMBINING ALL CONSTRAINTS

Let us now combine all constraints. This is done by a dedicated scan over $\hat{\boldsymbol{\alpha}}$ for each point in $\tan\beta$ and $M_{H^\pm}$. The value of χ^2 is determined as

$$\chi^2 = \chi^2_{\text{general}} + \sum_i \chi^2_i, \tag{5.1}$$

where χ^2_{general} is given by Eq. (3.19) and the sum runs over the observables R_b, LEP2 nondiscovery, $\Delta\rho$, and a_μ, all of them evaluated at the same point in $\hat{\boldsymbol{\alpha}}$. This quantity is then minimized over $\hat{\boldsymbol{\alpha}}$:

$$\hat{\chi}^2 = \min_{\hat{\boldsymbol{\alpha}} \in \boldsymbol{\alpha}_+} \chi^2, \tag{5.2}$$

for fixed $\tan\beta$ and $M_{H^\pm}$ and allowed regions are determined. In the $\tan\beta$-$M_{H^\pm}$ plane, the allowed regions will in general be less than the intersection of the regions that are allowed by the individual constraints. The reason is that the individual constraints may refer to different parts of the three-dimensional $\boldsymbol{\alpha}$ space.

We shall split this discussion into the two cases $\mu = 0$ and $M_1 < \mu$. In the former case, unitarity restricts the allowed range of $\tan\beta$, as illustrated in Fig. 1, whereas in the latter case also higher values of $\tan\beta$ are allowed.

A. Combining all constraints for $\mu = 0$

In Fig. 9 we display the 90% and 95% C.L. limits for $(M_1, M_2) = (100, 300)$ GeV and $(100, 500)$ GeV, in both cases for $\mu = 0$. For the case of moderately low $M_2 = 300$ GeV, we note that there is little additional exclusion, other than that due to the B-physics constraints and unitarity. The little extra is due to the $\Delta\rho$ constraint, at high values of $M_{H^\pm}$. However, for $M_2 = 500$ GeV, there is a considerable reduction of the allowed parameter space at $\tan\beta \gtrsim 1$–1.5. In this range of $\tan\beta$ values, we see from Fig. 5 (right panel), that high values of $M_{H^\pm}$ are excluded by the LEP2 nondiscovery constraint, and from Fig. 7 (right panel), we see that low values of $M_{H^\pm}$ are excluded by the $\Delta\rho$ constraint.

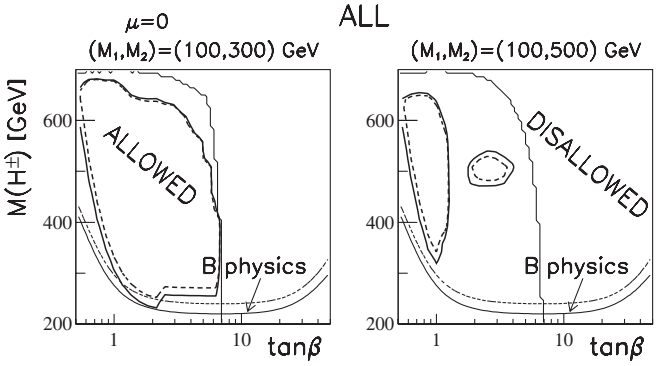

FIG. 9. Exclusions due to all constraints, for $(M_1, M_2) = (100, 300)$ GeV, and $(M_1, M_2) = (100, 500)$ GeV, both with $\mu = 0$. Heavy dashed: 90% C.L.; heavy solid: 95% C.L. Also shown is the region excluded by the B-physics constraints (thin dashed and solid), and the 0% contour from Fig. 1 (thin solid).

Similarly, Fig. 10 is devoted to the case $M_1 = 150$ GeV. In this case, the LEP2 nondiscovery plays no role, but there are of course also other differences, due to the way different parameters are correlated by the constraints. Overall, this case is less constrained than the $M_1 = 100$ GeV case of Fig. 8.

B. Combining all constraints for $M_1 < \mu$

When $M_1 < \mu$, the unitarity constraints no longer restrict $\tan\beta$ to low and moderate values. However, we shall see that various other constraints may cause a cutoff for large $\tan\beta$. For $M_1 = 100$ GeV and two values of M_2, namely, 300 GeV and 500 GeV, we display in Figs. 11–13 the allowed regions for a range of μ-values, from 200 GeV to 600 GeV.

For the lower value, $M_2 = 300$ GeV (left panels), the allowed region in the $\tan\beta$-$M_{H^\pm}$ plane is fairly extended, whereas for the higher value, $M_2 = 500$ GeV, it is more constrained, until μ reaches values comparable to M_2 (see the right panels of Figs. 11–13).

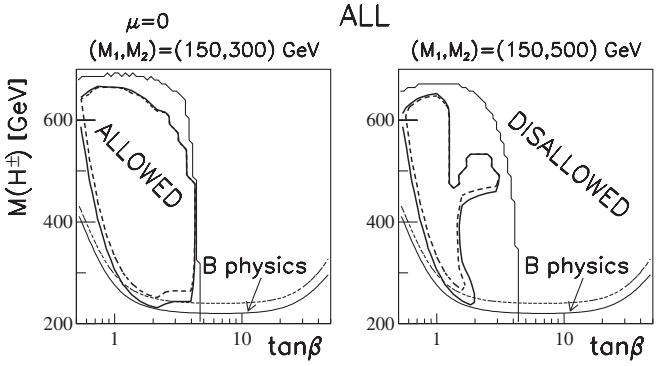

FIG. 10. Similar to Fig. 9, for $M_1 = 150$ GeV.

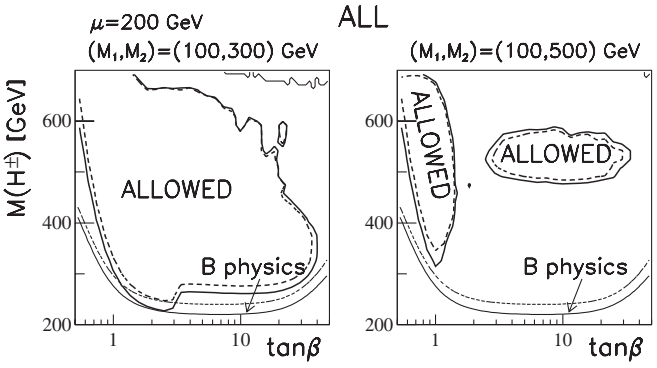

FIG. 11. Similar to Fig. 9, for $\mu = 200$.

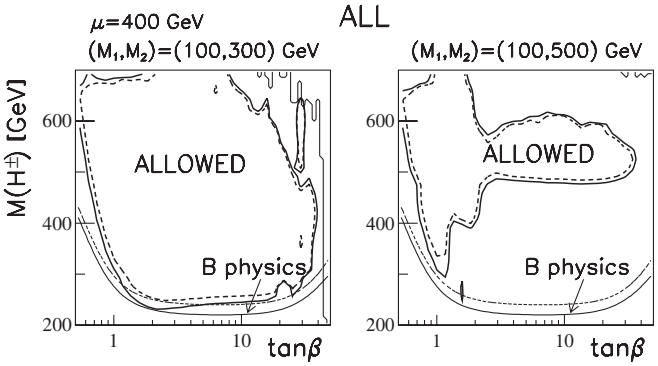

FIG. 12. Similar to Fig. 9, for $\mu = 400$.

For $\mu = 500$ GeV and $M_2 = 500$ GeV (not shown), the exclusion of low and high values of $M_{H^\pm}$ for $\tan\beta \gtrsim 2$ is due to the $\Delta\rho$ constraint, whereas the LEP2 nondiscovery by itself does not exclude anything in this case. However, the simultaneous imposition of the LEP2 nondiscovery and the $\Delta\rho$ constraints yields a "forbidden finger" at $\tan\beta \sim 1.5$ and low $M_{H^\pm}$, as well as some exclusion at low $\tan\beta$ and high $M_{H^\pm}$.

In all cases, we note that simultaneously high values of both $\tan\beta$ and $M_{H^\pm}$ are excluded, except when $M_2 < \mu$. This is due to the $\Delta\rho$ constraint, as discussed in Sec. IV C. For the cases shown ($M_1 = 100$ GeV), also the LEP2 non-

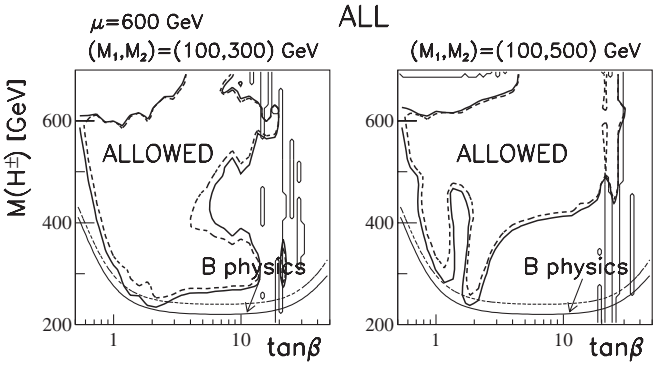

FIG. 13. Similar to Fig. 9, for $\mu = 600$.

discovery plays a role, but this will of course not have any impact for $M_1 > 114.4$ GeV.

VI. PROFILE OF SURVIVING PARAMETER SPACE

We shall here give a profile of the surviving parameter space in terms of three "hidden" parameters, α_1, α_2, and M_3. In discussing the surviving parameter space, we shall distinguish between low and high values of $\tan\beta$, giving some details relevant to $\tan\beta < 5$ and $\tan\beta > 10$.

A. Low values of $\tan\beta$

At low values of $\tan\beta$, both low and high values of μ lead to consistent solutions, with values of α_1 and α_2 distributed over extended regions of the parameter space, as shown in Fig. 14 for the case $\mu = 400$ GeV, $M_1 = 100$ GeV and two values of M_2, namely, 300 GeV and 500 GeV. (Further plots of this kind, but taking into account *only* the positivity and unitarity constraints, are presented in [18].)

We have here plotted the distributions of *all* α_1 and α_2 for which the total $\chi^2 < 5.99$ (see Eq. (5.1)), i.e., in general several points in (α_1, α_2) for each point in $(\tan\beta, M_{H^\pm})$.

At very low $\tan\beta$, an important constraint is the positivity of λ_2:

$$\lambda_2 = \frac{1}{s_\beta^2 v^2}[s_1^2 c_2^2 M_1^2 + (c_1 c_3 - s_1 s_2 s_3)^2 M_2^2 + (c_1 s_3 + s_1 s_2 c_3)^2 M_3^2 - c_\beta^2 \mu^2] > 0, \quad (6.1)$$

and the constraint from unitarity that it cannot become "large." For small μ, the M_3^2-term cannot be too large (in order not to violate unitarity). This requires

$$|c_1 s_3 + s_1 s_2 c_3| \ll 1. \quad (6.2)$$

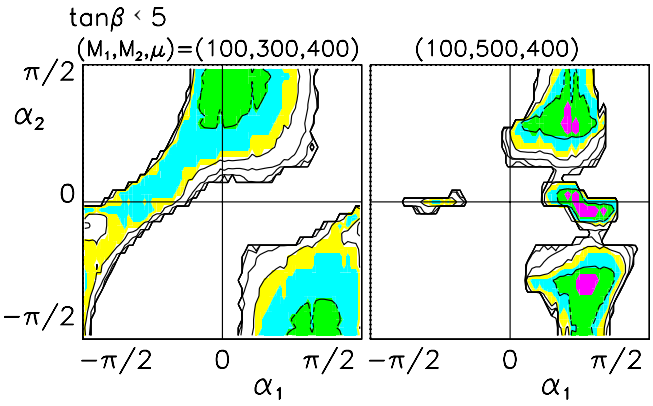

FIG. 14 (color online). Normalized distributions of allowed regions in the α_1-α_2 space, for low values of $\tan\beta$. Contours are shown at each negative power of 10, as appropriate. Yellow [light gray] (light blue) indicates where the normalized distribution is higher than 10^{-4} (3×10^{-4}); green (purple [darkest gray]) levels above 10^{-3} (3×10^{-3}). Along the lines $\alpha_2 = \pm\pi/2$, H_1 is CP-odd, and there is no CP violation.

As μ becomes large, with M_2 fixed, the M_3^2-term must compensate the μ^2-term, with $|c_1 s_3 + s_1 s_2 c_3| = \mathcal{O}(1)$. The distributions in Fig. 14 are seen to satisfy this condition.

While the allowed range of $M_{H^\pm}$ depends on the neutral-Higgs-boson mass M_2, it is typically of the order of 300–700 GeV. In most of the allowed parameter space, CP is violated, but along the edges $\alpha_2 \to \pm\pi/2$ there is no CP-violation. This is the limit where the lightest Higgs boson, H_1, becomes CP odd.

B. High values of $\tan\beta$

We show in Fig. 15 the populated regions in the α_1-α_2 plane, for $\mu = 400$ GeV and $\tan\beta > 10$. Two points are worth noting: (1) The allowed regions satisfy the constraints of (4.8). (2) The majority of points do *not* satisfy the condition (4.15), meaning that the $M_{H^\pm} \gg M_1$ case is not very relevant here. Instead, the degenerate case $\mu \sim M_{H^\pm} \sim M_2 \lesssim M_3$ is important, as also reflected in Table V part (c).

At high values of $\tan\beta$, μ has to be comparable to M_2, or higher. In particular, no solution exists for high values of $\tan\beta$ and $\mu = 0$. This is due to the unitarity constraints. Also, we note from Figs. 9–13, that unless μ is comparable to, or larger than M_2, the allowed range in $\tan\beta$ and $M_{H^\pm}$ can be rather limited. The range of $M_{H^\pm}$ depends on the neutral-Higgs-boson mass M_1, being typically of the order of 400–600 GeV. In order to understand the large-$\tan\beta$ parameter space, let us review

$$\lambda_1 = \frac{1}{c_\beta^2 v^2}[c_1^2 c_2^2 M_1^2 + (c_1 s_2 s_3 + s_1 c_3)^2 M_2^2 + (c_1 s_2 c_3 - s_1 s_3)^2 M_3^2 - s_\beta^2 \mu^2] > 0. \quad (6.3)$$

This should be positive, but not "too large." High values of μ require high M_3 and $|c_1 s_2 c_3 - s_1 s_3| = \mathcal{O}(1)$.

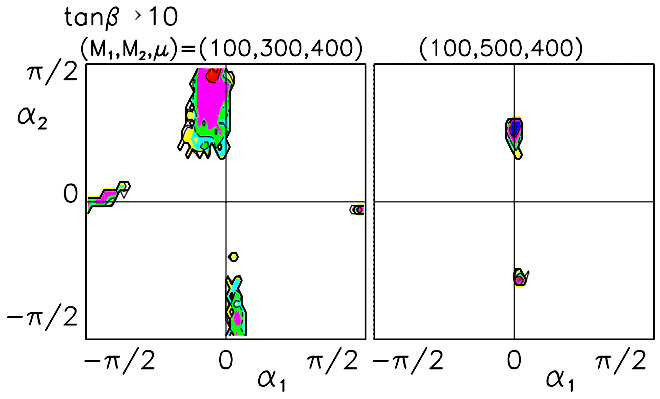

FIG. 15 (color online). Normalized distributions of allowed regions in the α_1-α_2 space, for high $\tan\beta$ values. Contours and color codes are as in Fig. 14, with additionally red (blue [darkest]) above 10^{-2} (3×10^{-2}).

TABLE V. Distribution of M_3 values, $\xi = M_3/M_2$.

[a]$\tan\beta$	$\xi < 1.1$	$1.1 < \xi < 1.5$	$1.5 < \xi$
$5-10$	94.6 [0.0]%	5.2 [0.0]%	0.2 [0.0]%
<5	43.4 [88.4]%	49.8 [11.6]%	6.8 [0.0]%

[b]$\tan\beta$	$\xi < 1.1$	$1.1 < \xi < 1.5$	$1.5 < \xi$
>10	74.0 [95.8]%	24.9 [4.2]%	1.0 [0.0]%
$5-10$	49.0 [91.4]%	48.4 [8.6]%	2.6 [0.0]%
<5	30.9 [81.5]%	56.8 [18.5]%	12.3 [0.0]%

[c]$\tan\beta$	$\xi < 1.1$	$1.1 < \xi < 1.5$	$1.5 < \xi$
>10	0.0 [91.6]%	69.0 [8.4]%	31.0 [0.0]%
$5-10$	0.0 [76.3]%	47.8 [23.7]%	52.2 [0.0]%
<5	0.0 [64.1]%	15.3 [35.8]%	84.7 [0.2]%

[d]$\tan\beta$	$\xi < 1.1$	$1.1 < \xi < 1.5$	$1.5 < \xi$
>10	0.0 [0.0]%	0.0 [93.8]%	100.0 [6.2]%
$5-10$	0.0 [0.0]%	0.0 [92.6]%	100.0 [7.5]%
<5	0.0 [0.0]%	0.0 [94.5]%	100.0 [5.6]%

[a]$\mu = 0$, $(M1, M2) = (100, 300[500])$ GeV.
[b]$\mu = 200$ GeV, $(M1, M2) = (100, 300[500])$ GeV.
[c]$\mu = 400$ GeV, $(M1, M2) = (100, 300[500])$ GeV.
[d]$\mu = 600$ GeV, $(M1, M2) = (100, 300[500])$ GeV.

C. Distribution of M_3

We recall that with our choice of parameters, the third neutral-Higgs mass is a derived quantity. The distribution of M_3 can be discussed in terms of the dimensionless ratio

$$\xi = \frac{M_3}{M_2}, \qquad 1 < \xi. \quad (6.4)$$

For three bins in ξ, this is for $\mu = 0$, 200, 400, and 600 GeV distributed as given in Table V. For $\mu = 0$, M_3 tends to be low, just marginally above M_2, as seen in Table V (a). This pattern is valid also for $M_1 < \mu$, provided only that $\mu < M_2$, see Table V parts (b) and (c). For $M_2 < \mu$, on the other hand, M_3 can be large.

D. The standard-model-like limit

The parameters of the 2HDM can be chosen such that the ZZH_1, bbH_1, and ttH_1 couplings all approach the corresponding SM values. This requires, in our notation [11]

$$\cos(\beta - \alpha_1)\cos\alpha_2 \simeq 1, \qquad \frac{\cos\alpha_1 \cos\alpha_2}{\cos\beta} \simeq 1, \qquad \frac{\sin\alpha_1 \cos\alpha_2}{\sin\beta} \simeq 1, \quad (6.5)$$

which is satisfied for $\beta \simeq \alpha_1$ and $\alpha_2 \simeq 0$. There could also be a "quasi-SM-like" limit, where one or more of the above quantities approaches -1 (denoted "Solution B" in [73]). For the familiar observables, such a sign change would not have any effect.

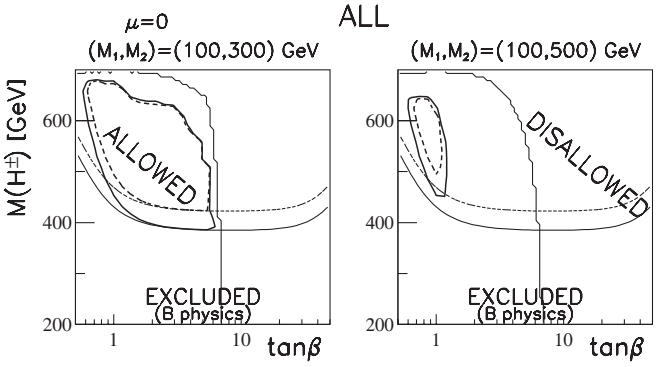

FIG. 16. Similar to Fig. 9, for $BR(\bar{B} \to X_s\gamma) = 3.20 \times 10^{-4}$ and an overall uncertainty $\sigma[\mathcal{B}(\bar{B} \to X_s\gamma)] = 0.25 \times 10^{-4}$ (c.f. Eq. (3.5)).

For $\tan\beta \lesssim 5$, the allowed regions in the α_1-α_2 space are rather extended, and SM-like solutions are found for a range of mass values. For $\tan\beta \gtrsim 10$, on the other hand, the populated parts of the α_1-α_2 space become very localized, and have the following features: (i) for $M_2 \gtrsim \mu$, $\alpha_1 \simeq 0$, and $|\alpha_2| > 0$, and (ii) for $M_2 \lesssim \mu$, additional regions emerge for small values of $|\alpha_2|$ and $|\alpha_1| \simeq \pi/2$. The latter, seen as small specks near the horizontal axis in the left panel of Fig. 15, correspond to the SM-like (and "quasi-SM-like") case.

For the case $M_1 = 100$ GeV, which is studied in most of our figures, there is of course a limit to how close we come to the SM limit, since a SM Higgs mass of this low value is excluded. Actually, the fact that for $(M_1, M_2) = (100, 500)$ GeV and $\mu = 0$, some region of the $\tan\beta$-$M_{H^\pm}$ plane is excluded by the LEP2 nondiscovery constraint (see right panel of Fig. 6), means that those regions correspond to solutions near the SM limit.

VII. POSSIBLE FUTURE CONSTRAINTS

It is interesting to see how the parameter-space constraints would be modified by possible future results from the B-physics sector. We shall not consider any change to the $\Delta\rho$ or LEP2 constraints, but rather discuss the possibility that the central value for the branching ratio for $\bar{B} \to X_s\gamma$ be reduced from 3.55×10^{-4} to 3.20×10^{-4}, a value closer to the SM prediction. Also changing the overall uncertainty to 0.25×10^{-4}, we find that the resulting constraints are significantly modified, as illustrated in Figs. 16 and 17 for $\mu = 0$ and 400 GeV, respectively.

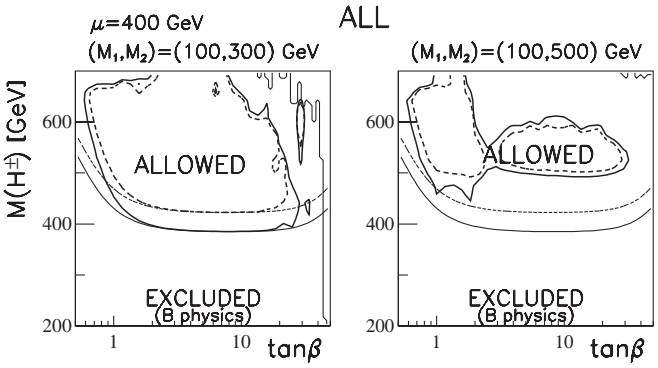

FIG. 17. Similar to Fig. 16, for $\mu = 400$ GeV.

VIII. SUMMARY

We have shown that the B-physics results, together with the precise measurement of the ρ-parameter at LEP and the constraint of tree-level unitarity of Higgs-Higgs scattering, exclude large regions of the 2HDM (II) parameter space. High values of $\tan\beta$ are excluded unless both M_2 and M_3 are heavy. Furthermore, they should be reasonably close to each other. Improved precision of the $\bar{B} \to X_s\gamma$ measurement could significantly reduce the remaining part of the parameter space, but it appears unlikely that the model could be excluded other than by a negative search at the LHC.

What is the corresponding situation for supersymmetric models? While the consistency then is guaranteed by internal relations, it should be kept in mind that light charged-Higgs bosons would be in conflict with the B-physics data unless some superpartner (for example, the chargino [74]) is also light. A possibility which has received some attention, is a light chargino and a light stop [75]. It has also been shown that anomalous effects at large $\tan\beta$ could weaken the bound on $M_{H^\pm}$ without light superpartners [76] (see also [77]). However, the more recent data on $B \to \tau\nu_\tau$ discussed in Sec. III B would presumably close this loophole (see Fig. 2 of [78]).

Similar scans over the parameter space of the constrained minimal supersymmetric standard model [79–81] differ from the present work in one major respect: they are required to yield an amount of dark matter that is compatible with the WMAP data [82]. Additionally, the a_μ constraint is more severe, due to one-loop contributions involving superpartners of the muon and muon neutrino. These studies are also more focused on the high-scale parameters, like m_0 and $m_{1/2}$, with less emphasis on $M_{H^\pm}$ and $\tan\beta$. The study by [80] shows a preference for positive μ (higgsino mass parameter, not to be confused with the μ of Eq. (2.1)), a relatively light charged-Higgs mass (a few hundred GeV) and rather high values of $\tan\beta$ ($\sim$ 50–60).

ACKNOWLEDGMENTS

It is a pleasure to thank Mikolaj Misiak for patiently explaining details of the $\bar{B} \to X_s\gamma$ calculation, and Andrzej Buras, Ulrich Jentschura, and Frank Krauss, for correspondence related to Ref. [59]. This research has been supported in part by the Mission Department of Egypt and the Research Council of Norway.

[1] T. D. Lee, Phys. Rev. D **8**, 1226 (1973).
[2] S. Weinberg, Phys. Rev. Lett. **37**, 657 (1976).
[3] G. C. Branco and M. N. Rebelo, Phys. Lett. B **160**, 117 (1985); J. Liu and L. Wolfenstein, Nucl. Phys. **B289**, 1 (1987); S. Weinberg, Phys. Rev. D **42**, 860 (1990); Y. L. Wu and L. Wolfenstein, Phys. Rev. Lett. **73**, 1762 (1994).
[4] E. Accomando *et al.*, arXiv:hep-ph/0608079.
[5] A. Riotto and M. Trodden, Annu. Rev. Nucl. Part. Sci. **49**, 35 (1999).
[6] M. Dine and A. Kusenko, Rev. Mod. Phys. **76**, 1 (2004).
[7] S. Bertolini, Nucl. Phys. **B272**, 77 (1986).
[8] A. K. Grant, Phys. Rev. D **51**, 207 (1995).
[9] K. Cheung and O. C. W. Kong, Phys. Rev. D **68**, 053003 (2003).
[10] N. G. Deshpande and E. Ma, Phys. Rev. D **18**, 2574 (1978); S. Nie and M. Sher, Phys. Lett. B **449**, 89 (1999); S. Kanemura, T. Kasai, and Y. Okada, Phys. Lett. B **471**, 182 (1999).
[11] A. W. El Kaffas, W. Khater, O. M. Ogreid, and P. Osland, Nucl. Phys. **B775**, 45 (2007).
[12] S. Kanemura, T. Kubota, and E. Takasugi, Phys. Lett. B **313**, 155 (1993).
[13] A. G. Akeroyd, A. Arhrib, and E. M. Naimi, Phys. Lett. B **490**, 119 (2000); A. Arhrib, arXiv:hep-ph/0012353.
[14] I. F. Ginzburg and I. P. Ivanov, arXiv:hep-ph/0312374; Phys. Rev. D **72**, 115010 (2005).
[15] J. F. Gunion, H. E. Haber, G. Kane, and S. Dawson, *The Higgs Hunter's Guide* (Addison-Wesley, Reading, MA, 1990).
[16] S. L. Glashow and S. Weinberg, Phys. Rev. D **15**, 1958 (1977).
[17] W. Khater and P. Osland, Nucl. Phys. **B661**, 209 (2003).
[18] A. W. El Kaffas, O. M. Ogreid, and P. Osland, arXiv:hep-ph/0702097 [Nonlin. Phenom. Complex Syst. (to be published)].
[19] O. Brein, Comput. Phys. Commun. **170**, 42 (2005).
[20] S. Bertolini, F. Borzumati, and A. Masiero, Phys. Rev. Lett. **59**, 180 (1987); N. G. Deshpande, P. Lo, J. Trampetic, G. Eilam, and P. Singer, Phys. Rev. Lett. **59**, 183 (1987).
[21] B. Grinstein and M. B. Wise, Phys. Lett. B **201**, 274 (1988); B. Grinstein, R. P. Springer, and M. B. Wise, Phys. Lett. B **202**, 138 (1988); Nucl. Phys. **B339**, 269 (1990).
[22] R. Grigjanis, P. J. O'Donnell, M. Sutherland, and H. Navelet, Phys. Lett. B **213**, 355 (1988); **286**, 413(E) (1992); G. Cella, G. Curci, G. Ricciardi, and A. Vicere, Phys. Lett. B **248**, 181 (1990); M. Misiak, Phys. Lett. B **269**, 161 (1991); H. Simma, Z. Phys. C **61**, 67 (1994); M. Ciuchini, E. Franco, G. Martinelli, L. Reina, and L. Silvestrini, Phys. Lett. B **316**, 127 (1993); M. Ciuchini, E. Franco, L. Reina, and L. Silvestrini, Nucl. Phys. **B421**, 41 (1994); G. Cella, G. Curci, G. Ricciardi, and A. Vicere, Phys. Lett. B **325**, 227 (1994); Nucl. Phys. **B431**, 417 (1994).
[23] A. J. Buras, M. Misiak, M. Munz, and S. Pokorski, Nucl. Phys. **B424**, 374 (1994).
[24] A. Ali and C. Greub, Z. Phys. C **60**, 433 (1993).
[25] M. Misiak, Nucl. Phys. **B393**, 23 (1993); **B439**, 461(E) (1995).
[26] K. Adel and Y. P. Yao, Phys. Rev. D **49**, 4945 (1994).
[27] C. Greub, T. Hurth, and D. Wyler, Phys. Lett. B **380**, 385 (1996); Phys. Rev. D **54**, 3350 (1996).
[28] K. G. Chetyrkin, M. Misiak, and M. Munz, Phys. Lett. B **400**, 206 (1997); **425**, 414(E) (1998).
[29] A. J. Buras, A. Kwiatkowski, and N. Pott, Phys. Lett. B **414**, 157 (1997); **434**, 459(E) (1998).
[30] M. Ciuchini, G. Degrassi, P. Gambino, and G. F. Giudice, Nucl. Phys. **B527**, 21 (1998).
[31] P. Gambino and M. Misiak, Nucl. Phys. **B611**, 338 (2001).
[32] A. J. Buras, A. Czarnecki, M. Misiak, and J. Urban, Nucl. Phys. **B631**, 219 (2002).
[33] H. M. Asatrian, C. Greub, A. Hovhannisyan, T. Hurth, and V. Poghosyan, Phys. Lett. B **619**, 322 (2005).
[34] V. D. Barger, J. L. Hewett, and R. J. N. Phillips, Phys. Rev. D **41**, 3421 (1990); S. Bertolini, F. Borzumati, A. Masiero, and G. Ridolfi, Nucl. Phys. **B353**, 591 (1991).
[35] M. Ciuchini, E. Franco, G. Martinelli, L. Reina, and L. Silvestrini, Phys. Lett. B **334**, 137 (1994).
[36] F. M. Borzumati and C. Greub, Phys. Rev. D **58**, 074004 (1998).
[37] M. Misiak *et al.*, Phys. Rev. Lett. **98**, 022002 (2007).
[38] M. Misiak and M. Steinhauser, Nucl. Phys. **B764**, 62 (2007).
[39] E. Barberio *et al.* (Heavy Flavor Averaging Group (HFAG)), arXiv:hep-ex/0603003.
[40] J. R. Andersen and E. Gardi, J. High Energy Phys. 01 (2007) 029; E. Gardi, arXiv:hep-ph/0703036.
[41] T. Becher and M. Neubert, Phys. Rev. Lett. **98**, 022003 (2007); Phys. Lett. B **633**, 739 (2006); **637**, 251 (2006).
[42] C. Bobeth, M. Misiak, and J. Urban, Nucl. Phys. **B574**, 291 (2000).
[43] M. Misiak and M. Steinhauser, Nucl. Phys. **B683**, 277 (2004).
[44] M. Czakon, U. Haisch, and M. Misiak, J. High Energy Phys. 03 (2007) 008.
[45] M. Gorbahn and U. Haisch, Nucl. Phys. **B713**, 291 (2005); M. Gorbahn, U. Haisch, and M. Misiak, Phys. Rev. Lett. **95**, 102004 (2005).
[46] I. Blokland, A. Czarnecki, M. Misiak, M. Slusarczyk, and F. Tkachov, Phys. Rev. D **72**, 033014 (2005); K. Melnikov and A. Mitov, Phys. Lett. B **620**, 69 (2005).
[47] T. van Ritbergen, Phys. Lett. B **454**, 353 (1999); K. Bieri, C. Greub, and M. Steinhauser, Phys. Rev. D **67**, 114019 (2003).
[48] P. Gambino and U. Haisch, J. High Energy Phys. 10 (2001) 020.
[49] J. Charles *et al.* (CKMfitter Group), Eur. Phys. J. C **41**, 1 (2005); M. Bona *et al.* (UTfit Collaboration), J. High Energy Phys. 10 (2006) 081.
[50] B. Aubert *et al.* (*BABAR* Collaboration), Phys. Rev. Lett. **93**, 011803 (2004).
[51] P. Koppenburg *et al.* (Belle Collaboration), Phys. Rev. Lett. **93**, 061803 (2004); A. H. Mahmood *et al.* (CLEO Collaboration), Phys. Rev. D **70**, 032003 (2004).
[52] T. Huber, E. Lunghi, M. Misiak, and D. Wyler, Nucl. Phys. **B740**, 105 (2006).
[53] C. W. Bauer, Phys. Rev. D **57**, 5611 (1998); **60**, 099907(E) (1999).
[54] M. Neubert, Eur. Phys. J. C **40**, 165 (2005).
[55] W. S. Hou, Phys. Rev. D **48**, 2342 (1993); Y. Grossman and Z. Ligeti, Phys. Lett. B **332**, 373 (1994); Y. Grossman, H. E. Haber, and Y. Nir, Phys. Lett. B **357**, 630 (1995).

[56] K. Ikado *et al.*, Phys. Rev. Lett. **97**, 251802 (2006); T. E. Browder, Nucl. Phys. B, Proc. Suppl. **163**, 117 (2007); B. Aubert (*BABAR* Collaboration), arXiv:hep-ex/0608019.

[57] L. F. Abbott, P. Sikivie, and M. B. Wise, Phys. Rev. D **21**, 1393 (1980); G. G. Athanasiu, P. J. Franzini, and F. J. Gilman, Phys. Rev. D **32**, 3010 (1985); S. L. Glashow and E. Jenkins, Phys. Lett. B **196**, 233 (1987); C. Q. Geng and J. N. Ng, Phys. Rev. D **38**, 2857 (1988); **41**, 1715(E) (1990).

[58] T. Inami and C. S. Lim, Prog. Theor. Phys. **65**, 297 (1981); **65**, 1772(E) (1981).

[59] J. Urban, F. Krauss, U. Jentschura, and G. Soff, Nucl. Phys. **B523**, 40 (1998).

[60] P. Ball and R. Fleischer, Eur. Phys. J. C **48**, 413 (2006).

[61] A. Abulencia *et al.* (CDF - Run II Collaboration), Phys. Rev. Lett. **97**, 062003 (2006); AIP Conf. Proc. **870**, 116 (2006).

[62] W. M. Yao *et al.* (Particle Data Group), J. Phys. G **33**, 1 (2006).

[63] M. Boonekamp, Eur. Phys. J. C **33**, S720 (2004); J. Abdallah *et al.* (DELPHI Collaboration), Eur. Phys. J. C **38**, 1 (2004).

[64] P. Achard *et al.* (L3 Collaboration), Phys. Lett. B **583**, 14 (2004).

[65] D. A. Ross and M. J. G. Veltman, Nucl. Phys. **B95**, 135 (1975); M. J. G. Veltman, Nucl. Phys. **B123**, 89 (1977); M. B. Einhorn, D. R. T. Jones, and M. J. G. Veltman, Nucl. Phys. **B191**, 146 (1981).

[66] G. W. Bennett *et al.* (Muon g-2 Collaboration), Phys. Rev. Lett. **92**, 161802 (2004); Phys. Rev. D **73**, 072003 (2006).

[67] A. Denner, R. J. Guth, W. Hollik, and J. H. Kuhn, Z. Phys. C **51**, 695 (1991).

[68] S. Schael *et al.* (ALEPH Collaboration, DELPHI Collaboration, L3 Collaboration, OPAL Collaboration, SLD Collaboration, LEP Electroweak Working Group, SLD Electroweak Group, and SLD Heavy Flavour Group), Phys. Rep. **427**, 257 (2006).

[69] F. Jegerlehner, arXiv:hep-ph/0703125.

[70] S. M. Barr and A. Zee, Phys. Rev. Lett. **65**, 21 (1990); **65**, 2920(E) (1990).

[71] D. Chang, W. F. Chang, C. H. Chou, and W. Y. Keung, Phys. Rev. D **63**, 091301 (2001).

[72] J. F. Gunion and H. E. Haber, Phys. Rev. D **67**, 075019 (2003).

[73] I. F. Ginzburg, M. Krawczyk, and P. Osland, arXiv:hep-ph/0101208; Nucl. Instrum. Methods Phys. Res., Sect. A **472**, 149 (2001).

[74] C. Bobeth, M. Misiak, and J. Urban, Nucl. Phys. **B567**, 153 (2000).

[75] R. Barbieri and G. F. Giudice, Phys. Lett. B **309**, 86 (1993); M. Ciuchini, G. Degrassi, P. Gambino, and G. F. Giudice, Nucl. Phys. **B534**, 3 (1998).

[76] G. Degrassi, P. Gambino, and G. F. Giudice, J. High Energy Phys. 12 (2000) 009.

[77] M. Carena, D. Garcia, U. Nierste, and C. E. M. Wagner, Phys. Lett. B **499**, 141 (2001).

[78] U. Haisch, arXiv:0706.2056.

[79] J. R. Ellis, S. Heinemeyer, K. A. Olive, and G. Weiglein, J. High Energy Phys. 05 (2006) 005.

[80] L. Roszkowski, R. R. de Austri, and R. Trotta, J. High Energy Phys. 07 (2007) 075.

[81] J. Ellis, S. Heinemeyer, K. A. Olive, A. M. Weber, and G. Weiglein, arXiv:0706.0652.

[82] D. N. Spergel *et al.*, Astrophys. J. Suppl. Ser. **170**, 377 (2007).